Nitric oxide mediates nitrite-sensing and acclimation and triggers a remodeling of lipids

Dolch, Lina-Juana; Lupette, Josselin; Tourcier, Guillaume; Bedhomme, Mariette; Collin, Séverine; Magneschi, Leonardo; Conte, Melissa; Seddiki, Khawla; Richard, Christelle; Corre, Erwan; Fourage, Laurent; Laeuffer, Frédéric; Richards, Robert; Reith, Michael; Rébeillé, Fabrice; Jouhet, Juliette; McGinn, Patrick; Maréchal, Eric

Publisher's version / Version de l'éditeur:
https://doi.org/10.1104/pp.17.01042
Plant Physiology, 175, 3, pp. 1407-1423, 2017-09-18

Title:

Nitric oxide mediates nitrite-sensing and adaptation and triggers a remodeling of glycerolipids in *Phaeodactylum*

Authors:

Lina-Juana Dolch[1], Guillaume Tourcier[1], Mariette Bedhomme[1], Séverine Collin[2], Leonardo Magneschi[1], Melissa Conte[1], Khawla Seddiki[1], Josselin Lupette[1], Erwan Corre[3], Dimitris Petroutsos[1], Laurent Fourage[2], Giovanni Finazzi[1], Fabrice Rébeillé[1], Juliette Jouhet[1], Robert Richards[4], Michael Reith[4], Patrick McGinn[4], Eric Maréchal[1,*]

Affiliations:

[1]Laboratoire de Physiologie Cellulaire et Végétale, Unité mixte de recherche 5168 CNRS - CEA - INRA - Université Grenoble Alpes, Institut de Biosciences Biotechnologies de Grenoble, CEA Grenoble, 17 rue des Martyrs, 38054, Grenoble Cedex 9, France.

[2]Total Refining Chemicals, Brussels, Belgium

[3]Station Biologique de Roscoff, Analyses and Bioinformatics for Marine Science, Roscoff, France

[4]National Research Council of Canada, Aquatic and Crop Resource Development, 1411 Oxford Street, Halifax, NS, Canada

* Correspondence: eric.marechal@cea.fr

Keywords:

Diatoms, *Phaeodactylum*, nitric oxide, nitrogen cycle, NOA, triacylglycerol

Abstract

Nitric oxide (NO) is an intermediate of the nitrogen cycle, an industrial pollutant and a marker of climate change. NO also acts as a gaseous transmitter in a variety of biological processes. The impact of environmental NO needs to be addressed. In diatoms, a dominant phylum in phytoplankton, NO was reported to mediate programmed cell death (PCD) in the model *Phaeodactylum tricornutum*, in response to 2E,4E/Z-decadienal (DD). Using the Pt1 strain, a higher susceptibility to DD was observed, leading to unspecific cellular membrane disruption. Production of NO in response to DD could not be observed. We re-examined NO biosynthesis and response in *Phaeodactylum*. NO inhibited cell growth and triggered triacylglycerol (TAG) accumulation. Feeding experiments indicate that NO is not enzymatically produced from arginine but *via* conversion of nitrite by a nitrate reductase (NR). Genome-wide transcriptional analysis show that NO upregulates the expression of the plastid nitrite reductase (NIR) and genes involved in the subsequent incorporation of ammonium into amino acids, *via* both glutamine synthesis and ornithine-urea pathway. The phosphoenolpyruvate dehydrogenase complex is also upregulated, leading to the production of acetyl-CoA, which can feed TAG accumulation upon non-transient exposure to NO. Transcriptional reprogramming leading to higher TAG content is balanced with a decrease of monogalactosyldiacylglycerol, *via* post-translational inhibition of MGD enzymatic activity by NO. A transient NO emission acts therefore at the basis of a nitrite-sensing and adapting system, whereas a non-transient exposure to NO can additionally induce a redirection of carbon to neutral lipids and a stress response.

Introduction

Nitric oxide ($NO^{\bullet}$) is an intermediate of the nitrogen (N) cycle (Fowler et al., 2013). This cycle is a complex network of reactions interconverting dinitrogen (N_2), the most abundant gas in the atmosphere, into gaseous nitrogen oxides or 'NOx' ($NO^{\bullet}$; nitrogen dioxide, NO_2 and nitrous gas, N_2O), water soluble anions (ammonium, NH_4^+; nitrite, NO_2^- and nitrate, NO_3^-), organic molecules (from small soluble compounds like urea to proteins, lipids and nucleic acids) and mineral forms (Holloway and Dahlgren, 2002; Fowler et al., 2013). $NO^{\bullet}$ is an important pollutant in industrial flue gases (Vunjak-Novakovic et al., 2005; Zhu et al., 2015) and wastewaters (Kampschreur et al., 2009; Pan et al., 2015). All gases in the N cycle, including $NO^{\bullet}$, are present in oceans (Zehr and Ward, 2002; Nicholls et al., 2007), either because of gas exchanges at the air-water interface (Nicholls et al., 2007) or because they are produced within oceans themselves. $NO^{\bullet}$ is generated in sea water by non-biological photochemical reactions (Olasehinde et al., 2010), large scale electrical discharges (Gallardo and Rhodes, 1997) and enzymatic activities in organisms living in the aerobic photic zone (Zhang et al., 2006; Olasehinde et al., 2010; Kumar et al., 2015; Eroglu et al., 2016) or in oxygen minimum zones (Naqvi et al., 1998; Nicholls et al., 2007; Martens-Habbena et al., 2015). Among the key biogeochemical cycles on which ecosystems depend for their sustainability, the N cycle is clearly the most perturbed by human activities (Fowler et al., 2013), marked by massive anthropogenic leakage of nitrate and ammonia from fertilized soils (Nicholls et al., 2007; Fowler et al., 2013) and by emissions of NOx (Nicholls et al., 2007; IPCC, 2014; Michalski et al., 2014).

There are no reliable reports on $NO^{\bullet}$ concentration in aquatic ecosystems because this reactive molecule has a lifetime of only a few seconds (Naqvi et al., 1998; Zehr and Ward, 2002; Zhang et al., 2006; Olasehinde et al., 2010). In natural seawater, $NO^{\bullet}$ concentration has been estimated between 0.01 and 10 nM (Zhang et al., 2006). In industrial microalgae cultivation systems supplied with industrial flue gas (Vunjak-Novakovic et al., 2005), we estimate that NOx/$NO^{\bullet}$ concentrations could reach the micro- to millimolar range, *i.e.* one thousand to one million fold above the natural level. $NO^{\bullet}$ diffuses freely and even minor and transient variations could have high impacts on living organisms, in which $NO^{\bullet}$ is also known to act as a signaling molecule.

$NO^{\bullet}$ has been reported to act as a gasotransmitter in a plethora of biological functions in prokaryotes and eukaryotes, in non-photosynthetic and photosynthetic cells and in terrestrial or aquatic ecosystems (Wendehenne et al., 2001; Moreau et al., 2010; Kumar et al., 2015; Eroglu

et al., 2016). Two major enzymatic pathways can produce NO• in aerobic conditions, either *via* a nitric oxide synthase (NOS) using arginine as a substrate (Wilson et al., 2008), or *via* a nitrate reductase (NR) using nitrite as a substrate (Yamasaki and Sakihama, 2000; Stohr et al., 2001; Rockel et al., 2002). The role of NO• in phytoplankton has been recently reviewed based on the available published data, showing that it could be synthesized in photosynthetic eukaryotes containing primary plastids (chlorophyta, rhodophyta) or secondary plastids (e.g. diatoms, haptophytes, etc.) (Kumar et al., 2015).

In the green alga *Chlamydomonas*, nitrite is assumed to be the only NO• source since the addition of arginine or the analogue Nω-Nitro-L-arginine had no effect on its production (Sakihama et al., 2002). NO• was shown to act on nitrogen assimilation, by repressing nitrate assimilation at two levels. Firstly, NO• represses the expression of the NR and the nitrate and ammonium transporters (de Montaigu et al., 2010). Secondly, it directly regulates the activities of NR and nitrate and ammonium transporters in *Chlamydomonas* (Sanz-Luque et al., 2013). Following nitrogen depletion of the medium , NO• was also shown to be produced from intracellular nitrite and to operate in the specific cytochrome b6f degradation pathway (Wei et al., 2014). In *Chlamydomonas*, NO• appears therefore to have a dual role, repressing nitrogen assimilation and acting in response to nitrogen starvation. In other photosynthetic eukaryotes, NO• may have opposing effects depending on the nitrogen status (Jin et al., 2009). To date, no clear scenario has arisen for a general model linking NO• signaling with the nitrogen status.

In the marine diatom *Phaeodactylum tricornutum*, NO• has been proposed to act in population size control, being involved in a "stress surveillance system" upon exposure to high concentrations of the diatom derived aldehyde 2E,4E/Z-decadienal (DD) (Vardi et al., 2006; Vardi et al., 2008). The treatment of *Phaeodactylum* with DD was reported (1) to induce a calcium spike followed by the synthesis of NO•, (2) to trigger the expression of the nitric oxide associated protein (*NOA*), coding for a homologue of a plant chloroplast protein involved in NO• production, and eventually (3) to promote the entry into programmed cell death (PCD) (Vardi et al., 2006; Vardi et al., 2008). The decrease in NO• produced by *Phaeodactylum* in the presence of a NOS-inhibitor led to the conclusion that NO• was produced by a NOS-like enzyme (Vardi et al., 2006), which seems contradictory with the absence of any *NOS* gene in the *Phaeodactylum* genome (Di Dato et al., 2015). NO• was therefore proposed to be derived from arginine and to act on the diatom itself, triggering PCD, and to diffuse outside the plasma

membrane, spread rapidly through diatom population, triggering death in surrounding cells, eventually acting in the control of the population size (Vardi et al., 2008; Bidle, 2015).

Climate change being marked by an increase in $NO^{\bullet}$ emissions, the biological perturbations it could create on phytoplankton has to be evaluated. *Phaeodactylum* appears as an appropriate model for this evaluation, firstly because the biosynthesis and physiological roles of $NO^{\bullet}$ have been previously investigated (Vardi et al., 2006; Vardi et al., 2008) and secondly because some diatom strains have been considered for biotechnological applications, based on their neutral lipid content (Levitan et al., 2014; Abida et al., 2015). In the present article, we analyzed the response of *Phaeodactylum* to various doses of $NO^{\bullet}$ and found unanticipated results that led us to re-examine the pathway of $NO^{\bullet}$-production by this diatom and the physiological responses this gasotransmitter could trigger.

Materials and methods

Chemicals

The chemicals used in the composition of growth media, the solvents as well as 3-[(3-cholamidopropyl)dimethylammonio]-1-propanesulfonate (CHAPS), 1,2-dioleoyl-sn-glycerol (DAG), 3-(N-morpholino)propanesulfonic acid (MOPS), nitroso acetyl penicillamine (NAP), S-nitroso-N-acetylpenicillamine (SNAP), phosphatidylglycerol (PG) and unlabeled uridine di-phosphogalactose (UDP-Gal) were obtained from Sigma-Aldrich. The fluorophore 4-amino-5-methylamino-2',7'-difluorescein diacetate (DAF-FM) was purchased from Thermofisher Scientific. The diatom derived aldehyde 2E,4E/Z-decadienal (DD) was obtained from Acros organics. [^{14}C]-labeled (11.0 GBq.mmol-1) UDP-Gal was obtained from New England Nuclear.

Cultivation of Phaeodactylum tricornutum

Phaeodactylum tricornutum (Pt1) Bohlin Strain 8.6 CCMP2561 (Culture Collection of Marine Phytoplankton, now known as NCMA: National Center for Marine Algae and Microbiota) was used in all experiments. Pt1 cells were maintained and grown in 20 mL or 50 mL at 20°C, in 250 mL flasks, in a modified ESAW (Enriched Seawater, Artificial Water) medium (NaCl 362.7 mM; Na_2SO_4 25 mM; KCl 8.03 mM; $NaHCO_3$ 2.067 mM; KBr 0.725 mM; H_3BO_3 0.372 mM; NaF 0.0657 mM; $MgCl_2$ 47.18 mM; $CaCl_2$ 9.134 mM; $SrCl_2$ 0.082 mM; Na_2-glycerophosphate 21.8 µM; Na_2SiO_3 105.6 µM; Na_2EDTA 14.86 µM; $Fe(NH_4)_2(SO_4)_2$ 5.97 µM; $FeCl_3$ 0.592 µM; $MnSO_4$ 2.42 µM; $ZnSO_4$ 0.254 µM; $CoSO_4$ 0.0569 µM; Na_2MoO_4 0.52 µM; H_3BO_3 61.46 µM; Na_2SeO_3 10 nM; biotin (vitamin H) 8.18 nM; cobalamin (vitamin B12) 2.94 nM; thiamine (vitamin B1) 0.594 µM) (Falciatore et al., 2000), using either ten times enriched nitrogen and phosphate sources ("10 x ESAW", containing 5.5 mM $NaNO_3$ and 0.22 mM NaH_3PO_4) (Abida et al., 2015) or the same medium without nitrogen. Cells were grown on a 12:12 light (30 µE $m^{-2}.sec^{-1}$) / dark cycle. Cells were sub-cultured twice a week by inoculating 1 x 10^6 cells mL^{-1} into fresh media. Growth was evaluated by cell counting using a Malassez counting chamber or by the absorption at 750 nm using a TECAN plate reader. For experiments in photo-bioreactors, cells were pre-cultured in a 50 mL volume of medium, in 250 mL Erlenmeyer flasks, until they reached a density of 2-4 x 10^6 cells mL^{-1}. Cells were then centrifuged at 3,500 g for 5 min and re-suspended in either 10 x ESAW or medium F (HEPES 100 mM, pH 7.5; NaCl 420 mM; $MgSO_4$ 5 mM; Na_2SO_4 3.5 mM; $CaCl_2$ 2.5 mM; $NaNO_3$ 70 mM; KH_2PO_4 0.88 mM; K_2HPO_4 2.3 mM; $NaHCO_3$ 10 mM; EDTA-Fe(III)-Na 0.11 mM; Na_2EDTA 0.18 mM; $ZnSO_4$ 4 µM; $CoCl_2$ 1.2 µM; $MnCl_2$ 15.5 µM; $CuSO_4$ 1.3 µM; biotin

(vitamin H) 0.1 µM; cobalamin (vitamin B12) 0.1 µM; thiamine (vitamin B1) 3.7 µM) (Benvenuti et al., 2015) to a final concentration of 2 x10^6 cells mL^{-1}. Cells were grown under a constant light regime at 20°C in small scale bioreactors (Multi-Cultivator MC 1000, Photon Systems Instruments, Czech Republic). Culture mixing throughout cultivation time was provided by gas sparging as in air-lift photobioreactors. A precise supply of CO_2 to the bioreactor tubes was controlled by the gas mixing system GMS 150 (Photon Systems Instruments, Czech Republic) following the manufacturer's instructions.

Incubation of* Phaeodactylum *with NO•-saturated solutions or NO•-donors

Incubation of *P. tricornutum* with gaseous NO• was performed by using NO•-saturated aqueous solutions. In this approach, a tank of pure NO• was bubbled into a small quantity of distilled water until the saturation point was reached, confirmed by mass spectrometric analysis of the solution. The concentration of NO• in a saturated solution was taken to be 1.9 mM (Gerrard, 1980). NO• saturates were then typically diluted 20-200 fold for use with live *Phaeodactylum* suspensions. Alternatively, a NO•-donor agent, S-Nitroso-N-acetylpenicillamine (SNAP) was used. This compound releases NO• when dissolved (Miller and Megson, 2007) and was therefore prepared freshly immediately before use. Nitroso-acetylpenicillamine (NAP) was used as a non-active compound for control experiments.

Incubation of* Phaeodactylum *with the diatom derived aldehyde DD

Since DD is a highly toxic and volatile compound, all experiments were performed under a fume hood safety cabinet and only freshly prepared DD solutions were used, either solubilized in dimethylsufoxide (DMSO) or in the growth medium. A 500 µL volume of a *Phaeodactylum* culture was inoculated at a cell density of 2 x 10^6 cell mL^{-1} and after a 24 hour-preincubation under gentle agitation, cells were treated with different concentrations of DD (DMSO, 0.5% final concentration). Untreated and treated cells were then observed by confocal microscopy, using the 680 nm fluorescent filter allowing chlorophyll detection. Relative fluorescence at 680 nm was quantified using a TECAN infinite M1000Pro plate reader.

Measure of nitric oxide using DAF-FM, a fluorescent reporter molecule

The fluorophore 4-amino-5-methylamino-2',7'-difluororescein diacetate (DAF-FM) allows the sensitive detection of low levels of nitric peroxide ($ONOO^-$), which is in equilibrium with NO• and thus indicates NO• levels (St Laurent et al., 2015). DAF-FM was previously used to detect NO• levels in *P. tricornutum* cells (Vardi et al., 2008). Cultures were diluted to obtain 10^6 cells

mL^{-1} in 10 mL and cells were incubated under gentle shaking with 20 µL of 5mM DAF-FM (in DMSO) for 1.5 hours, at room temperature and in the dark. Cells were washed and resuspended in 10 mL of fresh 10 x ESAW medium. Aliquot fractions (500 µL) were transferred to a 48 well culture plate, to which SNAP was added as indicated. For the examination of DAF-FM-dependent detection of nitric peroxide, 150 µL samples were transferred into a 96 well plate and fluorescence was measured with a TECAN infinite M1000Pro plate reader (excitation wavelength at 488 nm, emission at 529 nm).

Fast chlorophyll fluorescence kinetics measurements

To determine photosynthesis parameters in cell cultures, room temperature fast chlorophyll fluorescence kinetics were measured using a Speedzen MX fluorescence imaging system (JBeamBio) with settings previously described (Allorent et al., 2013). To this end, a 150 µL volume of *P. tricornutum* culture was transferred to a transparent 96 well-plate and dark-incubated for 15-30 min before measurements. Excitation was performed in the blue range (λ = 450 nm, *F0*) and actinic light pulses were given with a photosynthetic active wavelength of 520 nm. *F0* is the steady state fluorescence in dark-adapted cultures, *F* in light-adapted cultures; *Fm* is the maximal fluorescence after a saturating light pulse of dark-adapted cultures, *Fm'* the same in light adapted cultures, *Fv* is the difference between *F0* and *Fm*. With these parameters, the maximum efficiency of energy conversion by photosystem II (PSII) can be calculated as *Fv/Fm* (Misra et al., 2012).

Measure of triacylglycerol accumulation by Nile Red staining

Accumulation of triacylglycerol droplets was monitored by Nile Red (Sigma Aldrich) fluorescent staining (excitation wavelength at 485 nm; emission at 525 nm) as previously described (Cooksey et al., 1987; Abida et al., 2015). In brief, cells were diluted and adjusted to a cell density that was linearly correlated with Nile Red fluorescence. Nile Red solution (40 µL of a 2.5 µg mL^{-1} stock solution in DMSO) was added to 160 µL cell suspensions. Oil bodies stained with Nile Red were then visualized using a Zeiss AxioScope.A1 microscope (FITC filter; excitation wavelength at 488 nm; emission at 519 nm). The productivity, corresponding to the accumulation of TAG per volume and per time unit was calculated based on the staining by Nile Red, and expressed in relative fluorescence unit (Rfu) of Nile Red per mL and per day of incubation. Alternatively, Nile red fluorescence values were normalized to the cell concentration.

Genetic construction for NOA overexpression.

Genomic DNA was extracted from *Phaeodactylum tricornutum* Pt1 cells using the following procedure. Firstly, 10^8 cells were harvested and frozen in liquid nitrogen. A volume of 20 µL of Edward-Buffer (Tris-HCl 200 mM, pH 7.5; NaCl 250 mM; EDTA 25 mM; SDS 0.5%, w/v) was added, then samples were homogenized and debris removed by centrifugation. The supernatant was transferred to the same volume of isopropanol to precipitate DNA. After an additional 15 minute centrifugation at 10,000 x g, the pellet was washed with ethanol 70%, dried and solubilized in TE buffer (10 mM Tris-HCL pH7, 1 mM EDTA). DNA concentration was measured using a Nanodrop 2000 spectrophotometer (Thermo Scientific). Using genomic DNA as matrix, a 2,352-bp sequence was amplified by polymerase chain reaction (PCR) with the following oligonucleotides designed from Phatr2_56150 (Vardi et al., 2008) and carrying respectively *Xba*I and *EcoR*I restriction sites (underlined sequence): NOA-Fw *Xba*I 5'-TTTATCTAGAATGGTCCCCACTGGTTGTATG-3', NOA-Rev *EcoR*I 5'-TTTAGAATTCCTAATTACGCCCTACACCTTTTCTTC-3'. The gene ID of NOA in the third version of the genome (http://protists.ensembl.org/Phaeodactylum_tricornutum) is Phatr3_J40200. PCR was performed using Phusion High Fidelity polymerase (Thermo Scientific) according to the manufacturer's instructions. The PCR product was digested by *EcoR*I and *Xba*I, purified and cloned in the linearized expression vector. The expression vector used for overexpression corresponds to the pH4-GUS vector (De Riso et al., 2009). The vector contains a gene coding for resistance to zeocin (Shble), allowing selection of transformed cells. Expression of the NOA gene is controlled by the constitutive histone 4 promoter.

Transformation of* Phaeodactylum *and selection of strain overexpressing NOA.

Wild type *Phaeodactylum tricornutum* cells were transformed *via* particle-bombardment under aseptic conditions (Kikkert, 1993), using a protocol described previously (Falciatore et al., 1999) modified as follows. A three to four day-old Pt1 culture was concentrated to 4 x 10^7 cells in 500 µL and spread onto a 1% agar-plate containing 1 x ESAW medium. While shaking vigorously, 2-3 µg of non-linearized plasmid were added to 25 µL ethanol-sterilized tungsten particles (Sigma), together with 25 µL of 2.5 M $CaCl_2$ and 10 µL of 0.1 M spermidine. After mixing for three minutes using a vortex, the pellet was washed two times (1,500 g; 5 sec; room temperature) with 700 µL precooled 100% ethanol. DNA-coated tungsten particles were then resuspended in 25 µL 100% ethanol. A 12 µL fraction of the mix was transferred onto a macrocarrier and bombardment was carried out using 1,550 psi rupture disks (BioRad). After two to three days of incubation under continuous illumination, cells were transferred to similar agar-plates containing 100 µg mL^{-1} zeocin (Promega) for the selection of resistant transformed

cells. Colonies appearing after 4 to 6 weeks were transferred to a new plate for one week, prior to inoculation of 20 mL-liquid cultures.

Analysis of NOA gene expression in* Phaeodactylum tricornutum *cells.

To quantify the *NOA* mRNA level in overexpressing lines, quantitative polymerase chain reaction (qPCR) was performed after reverse transcription (RT) of extracted RNA. RNA was extracted from 10^7 cells that were previously pelleted, frozen in liquid nitrogen and stored at -80 °C until processing. A volume of 1 mL TriReagent (Sigma) was added to the frozen pellet and transferred to a new Eppendorf tube. After mixing for 30 sec using a vortex, samples were incubated for 5 min at room temperature. Chloroform (200 µL) was added and tubes, inverted and incubated for 15 min at room temperature. Phase separation was achieved by centrifugation (1,500 g; 30 min; 4°C). The upper phase was transferred to a new tube and RNA was precipitated using 1 volume isopropanol (1,500 g; 30 min; 4°C), washed with 75 % ice cold ethanol (1,500 g; 5 min; 4°C) and the pellet was dried in a Speed Vac system (Eppendorf Concentrator 5301) prior to suspension in 30 µL diethyl dicarbonate (DEPC) treated water (Sigma) at 65 °C for 10 min. RNA was purified following a second ethanol precipitation using 1 volume of 5 M ammonium, acetate (2.5 M final concentration) and 1 volume isopropanol. Samples were incubated for 10 min on ice and centrifuged, washed, dried and re-suspended as above. Concentration was determined using a NanoDrop device (Thermo Scientific). The RNA obtained (1 µg) was used for reverse transcription after DNAse treatment (Qiagen) following manufacturer's instructions so as to yield 1 µg cDNA, which were diluted to 10 ng μL^{-1}. For quantitative real time PCR, housekeeping gene oligonucleotides previously described (Siaut et al., 2007), namely *RPS* (5′-CGAAGTCAACCAGGAAACCAA-3′ and 5′-GTGCAAGAGACCGGACATACC-3′) and *TUBA* (5′-CTGGGAGCTTTACTGCTTGGA-3′ and 5′-ATGGCTCGAGATCGACGTAAA-3′), were used as internal controls. *NOA*-specific oligonucleotides were 5'-CCTGAAAAGTTCGCTACGCA-3' and 5'-CGGATCCTTTTTGCCCTGAG-3'. The total qPCR reaction volume was 10 µL (120 nM oligonucleotide, 20 ng cDNA, 5 µL 2X SYBR Green Sso Advanced (BioRad)). A two-step thermo-profile in 40 cycles was applied after 3 min at 95 °C initial denaturation (95°C for 10 sec; 58°C for 30 sec) and a melt curve was detected (from 65°C to 95 °C with a 0.5 °C increment) (BioRad CFX Connect Real-Time System). Evaluation of gene expression was carried out in 3 biological replicates, each one with technical triplicates, using the CFX Connect Real-Time System software, with *TUBA* and *RPS* as internal controls.

Lipidomic profiling by liquid chromatography – tandem mass spectrometry

Glycerolipids were extracted from freeze-dried *P. tricornutum* cells grown in 50 mL of medium. About 50 x10^6 to 100 x10^6 cells are required for a triplicate analysis. First, cells were harvested by centrifugation and immediately frozen in liquid nitrogen. Once freeze-dried, the pellet was suspended in 4 mL of boiling ethanol for 5 minutes to prevent lipid degradation, and lipids were extracted as described previously (Simionato et al., 2013) by addition of 2 mL methanol and 8 mL chloroform at room temperature. The mixture was then saturated with argon and stirred for 1 hour at room temperature. After filtration through glass wool, cell debris was rinsed with 3 mL chloroform/methanol 2:1, v/v, and 5 mL of 1% NaCl were then added to the filtrate to initiate phase separation. The chloroform phase was dried under argon before solubilizing the lipid extract in 1 mL of chloroform. Total glycerolipids were quantified from their fatty acids (FAs): in a 10 µL aliquot fraction a known quantity of saturated 15-carbon FA (15:0) was added and all FAs were methanolyzed into methyl esters (FAME) by a 1 hour incubation in 3 mL 2.5% H_2SO_4 in pure methanol at 100°C (Jouhet et al., 2003). The reaction was stopped by addition of 3 mL water, and 3 mL hexane were added for phase separation. After 20 min of incubation, the hexane phase was transferred to a new tube. FAMEs were extracted a second time via the addition, incubation and extraction of another 3 ml hexane. The combined collected hexane fractions (6 ml) were argon-dried and FAMEs were suspended in 30 µL hexane for analysis by gas chromatography coupled with flame ionization detection (GC-FID) (Perkin Elmer), using a BPX70 (SGE) column. FAMEs were identified by comparison of their retention times with those of standards (Sigma) and quantified by the surface peak method using 15:0 for calibration. Extraction and quantification were performed with at least three biological replicates. Glycerolipids were then analyzed and quantified by high pressure liquid chromatography-tandem mass spectrometry (HPLC-MS/MS), with appropriate standard lipids. For a technical triplicate analysis of TAG, an aliquot of the lipid extract containing 25 nmol of total FAs was dried under argon and dissolved in 100 µL of a methanol/chloroform solution (1:2) containing 125 pmol of 18:0/18:0/18:0 TAG as internal standard. For each replicate, 20 µL were injected in the HPLC-MS/MS system. The analytical device comprised an LC system with binary pumps (Agilent 1260 Infinity) coupled to a QQQ MS (Agilent 6460) equipped with a JetStream electrospray vane of injection. TAGs were separated by HPLC from other lipids using a diol column (Macherey-Nagel, EC 150/2 Nucleosil 100-5 OH) maintained at 40°C. Chromatography was performed using two solvents, i.e. solvent A (isopropanol/water/ammonium acetate 1 M pH 5.3 (850:125:1, v/v) and solvent B (hexane/isopropanol/water/ammonium acetate 1 M pH 5.3 (625:350:24:1, v/v)) and the following gradient: from 0 to 5 min, 100% B; from 5 to 30 min, a linear increase of A to 100%;

from 30 to 45 min, 100% A; from 45 to 50 min, a linear increase of B to 100%, and from 50 to 70 min, 100% B. The various glycerolipid species were detected from their *m/z* ratio by MS/MS using the Multiple Reaction Monitoring (MRM) mode. The various transition reactions used to identify the different glycerolipid species are those previously established with *Phaeodactylum tricornutum* (Abida et al., 2015). Quantification was made using the Agilent Mass Hunter software furnished by the MS supplier.

MGDG synthase enzymatic assay

A culture of *Phaeodactylum tricornutum* (50 mL in 10 x ESAW medium) was arrested in exponential phase and protein concentration determined using the Lowry method (Lowry et al., 1951). Cells were harvested by a centrifugation for 10 min at 1,500 x g at 4°C. The pellet was resuspended in 1 volume of 12mM 3-[(3-cholamidopropyl)dimethylammonio]-1-propanesulfonate (CHAPS) and 20 mM 3-(N-morpholino)propanesulfonate-KOH (MOPS-KOH), pH 7.8 and incubated for 20 minutes at 4°C to solubilize membrane proteins. Detergent solubilized proteins (10 µg) were then incubated for 1 hour with variable concentrations of SNAP (from 0 to 2 mM, as indicated) at room temperature in the dark in a final volume of 66.5 µL. After incubation with SNAP, galactosyltransferase enzyme activity was assayed in mixed micelles at 25°C, as described previously (Marechal et al., 1994). Phosphatidylglycerol (1.3 mM) and 1,2-dioleoyl-sn-glycerol (160 µM) dissolved in chloroform were first introduced into clean glass tubes. After evaporation of chloroform under a stream of argon, 300 µL of incubation medium adjusted to contain 10 µg proteins, 6 mM CHAPS, 250 mM KCl, 250 mM KH_2PO_4/K_2HPO_4 and 10 mM MOPS-KOH pH 7.8 were added. The mixture was mixed vigorously and kept 1 hour at 25°C for equilibration of mixed micelles. The reaction was then started by addition of 1 mM UDP-[^{14}C]Gal (37 Bq.µmol^{-1}) and stopped after 20 min by addition of chloroform/methanol (1:2, v/v). The lipids were subsequently extracted (Bligh and Dyer, 1959) and the radioactivity of the [^{14}C]-labeled MGDG produced, determined by liquid scintillation counting. Activity is expressed in nmol incorporated galactose h^{-1} mg protein^{-1}.

RNAseq analysis.

An actively growing stock culture of *Phaeodactylum* tricornutum was used to inoculate duplicate 100 mL experimental cultures in 250 mL Erlenmeyer flasks at an initial cell density of 2 x 10^6 cells mL^{-1}. Using a calibrated saturated NO$^\bullet$ solution, single additions at the start of the experiment were made to treated cultures to produce initial concentrations of either 3 or 10 µM NO$^\bullet$. Untreated cultures received no NO$^\bullet$. Cultures were allowed to grow for 4 days before

harvesting cells by centrifugation at 5000 rpm for 15 minutes at room temperature. After discarding the supernatant, cell pellets were flash frozen in liquid nitrogen and stored at -80° C before processing. In brief, cell aliquots were processed individually by grinding in liquid nitrogen in a mortar and pestle followed by extraction in RNA Pro lysis solution (MP Biomedicals) using a FastPrep homogenizer (two 40-sec cycles, with power set at level 6, following manufacturer instructions). After centrifugation, the supernatant was recovered and extracted with chloroform; RNA was precipitated by addition of an equal volume of cold absolute ethanol and incubation at -20°C overnight. Precipitated RNA was recovered by centrifugation, washed in 75% ethanol and air dried. The pellet was dissolved in RNase-free water and further purified using the clean-up protocol for the Qiagen RNeasy Mini Kit. RNA samples were quantified with a NanoDrop spectrophotometer and analyzed on an Agilent BioAnalyzer using the Plant RNA Nano program. 2.5 µg of each RNA was sent for RNA-Seq analysis at the McGill University and Genome Quebec Innovation Centre. Libraries for each sample were prepared for stranded 100 bp paired end sequencing and samples were combined and analyzed in a single Illumina Hiseq 2000 lane. Reads were mapped on the most recent genome version of *Phaeodactylum tricornutum* (http://protists.ensembl.org/Phaeodactylum_tricornutum) using the Star (Spliced Transcripts Alignment to a Reference) method (Dobin et al., 2013; Engstrom et al., 2013). Data were filtered based on the detection of 1 read in at least one sample per treatment or genomic mutation and then normalized using the DESseq2 method (Varet et al., 2016). Only genes being differentially expressed with a |Log2(fold change)| > 1 in at least one of the contrasts (i.e. comparing $NO^{\bullet}$ supplies at 0 µM vs. 3 µM, 0 µM vs. 10 µM or 3 µM vs. 10 µM), and with p-value lower than 0.05, were considered for further analyses. A partition of differentially expressed genes was performed using a K-mean method, with a number of partitions set to 6 and a clustering based on a Euclidian distance (Liu et al., 2014). For each group we sought whether gene ontology (GO) terms could be enriched, either by the DAVID method (http://david.abcc.ncifcrf.gov) (Huang et al., 2007), using the corresponding Refseq gene IDs and with a p-value threshold set at 0.1, or using the GOseq R package (Young et al., 2010) with an identical p-value threshold. Based on GO enriched terms, a focused analysis of acyl-lipid pathways and of nitrogen assimilation was performed, using a list of gene sequences with curated annotations.

Results and Discussion

Treatment of *P. tricornutum* with 2E,4E/Z-decadienal leads to cell necrosis and does not allow the detection of NO• production

We started our study by setting up an experimental protocol previously reported to enable the measurementof NO• production by *P. tricornutum* in response to putative infochemicals deriving from disrupted diatoms cells (Vardi et al., 2006; Vardi et al., 2008). Following wounding or nutrient stresses, diatom polyunsaturated fatty acids are oxidized enzymatically into volatile polyunsaturated aldehydes (PUAs), *i.e.* 2E,4Z,7E-decatrienal and 2E,4E-decadienal (DD) (Miralto et al., 1999), shown to impair grazer's reproduction (Ianora and Miralto, 2010). PUAs have been considered as potent interspecific and intraspecific signaling compounds (Casotti et al., 2005; Vardi et al., 2006). By treating *P. tricornutum* and *Thalassiosira weissflogii* with increasing doses of DD from 33 to 66 µM, a burst of NO• was measured using DAF-FM as a NO•-reporter, appearing within 5 minutes, with an intensity proportional to DD concentration (Vardi et al., 2006). Both DD and externally provided NO• were then reported to trigger programmed cell death (PCD). Production of NO• and PCD were blocked by N(G)-monomethyl-L-arginine, supporting an arginine-dependent production by a NOS-like enzyme. The threshold concentration of DD required to induce PCD was ~20 µM (Vardi et al., 2006).

We sought therefore to detect the endogenous biosynthesis of NO• in *Phaeodactylum* wild type (WT) cells, following treatment with supposedly non-lethal doses of DD, set at 3.3 µM and 10 µM (Vardi et al., 2006; Vardi et al., 2008). However, after 30 min incubation, the relative chlorophyll fluorescence normalized to the cell concentration was reduced by 50 % and further decreased with time compared to untreated controls (Figure S1A). The *Fv*/*Fm* ratio dropped immediately after addition of DD, with a strong decrease of fluorescence in dark-adapted cultures (*F0*) that correlated with chlorophyll concentrations. The *Fv/Fm* ratio relaxed over time, recovering its initial level (Figure S1B). Concomitantly, cell growth was arrested following DD treatment (Figure S1C). The discrepancy of chlorophyll decrease but artifact *Fv*/*Fm* recovery suggested a disruption of the chloroplast limiting membranes. This was confirmed by confocal imaging showing a disintegration of *Phaeodactylum* chloroplasts in response to DD (Figure S1D), consistent with the known unspecific membrane disrupting property of PUAs (Ribalet et al., 2007). The destructive effect of DD was similar if it was added directly to the culture or from a stock solutions dissolved in DMSO (final concentration 0.5%).

We treated cells with lower doses and found a similar response at concentrations ranging from 100 nM to 3.3 µM DD (Figure S2). Even at 100 nM, the *Fv/Fm* measures were already half of that of untreated cells (Figure S2). The sensitivity of *Phaeodactylum* to DD was therefore much higher than previously published (Vardi et al., 2006; Vardi et al., 2008). We could not detect any evidence for a PCD induced by DD exposure, but rather a non-specific necrosis. In *Phaeodactylum*, the cellular level of polyunsaturated fatty acids (mainly eicosapentaenoic acid, EPA) is about 2 nmol per 10^6 cells in nutrient replete or nitrogen- or phosphorus-deprived media (Abida et al., 2015). Supposing that all EPA could be converted into PUAs, one should consider that 5 x10^6 *Phaeodactylum* cells per mL should be lysed to reach 10 µM PUAs (the level of DD used here), and at least 1.65 x 10^7 to 3.3 x 10^7 lysed cells per mL to reach 33 and 66 µM PUAs (levels of DD in previous studies) (Vardi et al., 2006). These cell concentrations are far above those used here, by at least three orders of magnitude, and indeed the most recent survey of PUA levels in oceans shows that the highest concentration was in the nanomolar range (Ribalet et al., 2014). Thus, although we could not confirm that DD could act as a cell-to-cell specific signal in a sub-micromolar concentration range, we do not exclude that it could play this role within a physio-ecological concentration, *i.e.* in the pico- to nanomolar range, and future work should therefore re-address this question.

The cPTIO reagent (carboxy-2-phenyl-4,4,5,5-tetramethyl-imidazoline-1-oxyl-3-oxide) donates an oxygen atom to generate NO_2 and is often used to scavenge $NO^{\bullet}$ and act as an antidote (Keszler et al., 2010). We sought to determine whether DD-treated cells could be rescued by cPTIO, as previously reported (Vardi et al., 2008). Unexpectedly, *Phaeodactylum* cells proved to be highly sensitive to cPTIO as well, with a one third decrease of chlorophyll and a 20% decline in *Fv/Fm* after incubation with 100 µM cPTIO (dissolved in ESAW) (Figure S3). Cytotoxic effect of PTIO was also observed (not shown). Therefore, in the following experiments, neither cPTIO nor PTIO could be used to revert the effects observed after $NO^{\bullet}$ treatments. In addition, whereas the caspase/metacaspase inhibitor carbobenzoxy-valyl-alanyl-aspartyl-[O-methyl]-fluoromethylketone (Z-VAD-FKM) had been stated to partly rescue *Phaeodactylum* treated with DD (Vardi et al., 2008), we could not detect any effect of Z-VAD-FKM supplied at 20 to 40 µM on cells treated with 3.3 µM DD (not shown). Taken together, we could not obtain results consistent with a specific DD → PCD cascade. We therefore reconsidered the complete question of the physiological role of $NO^{\bullet}$.

External supply of $NO^{\bullet}$ impairs the growth of *P. tricornutum*

We used two differentmethods for supplying nitric oxide, either by providing NO• directly to the cells through the additions of dilutions of an NO•-saturated solutionor by adding a NO•-donor agent, S-Nitroso-N-acetylpenicillamine (SNAP). Nitroso-acetylpenicillamine (NAP), a structural analog of SNAP which lacks the NO-moiety, was used as a control for SNAP experiments. We verified the production of NO• following SNAP dissolution by two methods. Firstly, using Membrane Inlet Mass Spectrometry (MIMS, NRC Halifax laboratories), we observed an increase of the NO• signal (*m/z* = 30) with increasing doses of SNAP, up to a concentration of 600 µM (Figure S4A). Secondly, using the DAF-FM probe, we detected a signal in less than 30 minutes following dilution (Figure S4B), showing the efficiency of this NO•-donor in our experimental design. Both NO• donated by SNAP (Figure 1A) or supplied directly as a gas (not shown) impaired the growth of *Phaeodactylum*, as previously reported (Vardi et al., 2006; Vardi et al., 2008). A concentration of 1 mM SNAP reduced growth by only 20%, and was selected for further experiments. In contrast to DD, SNAP treatment did not affect chlorophyll levels (Figure 1B).

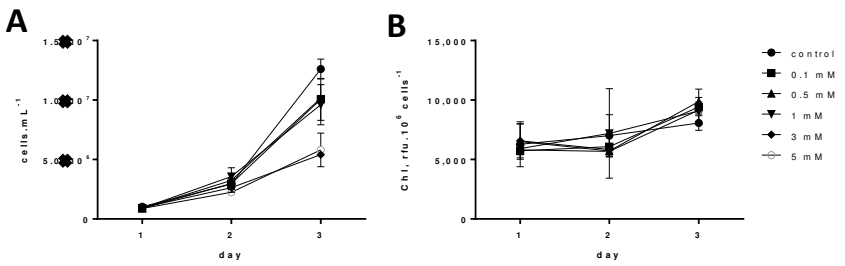

Figure 1: Effect of NO• supplied by SNAP on the growth of *Phaeodactylum*. The incubation was performed in a volume of 500 µL, inoculated at 10^6 cells.mL^{-1}, with immediate addition of SNAP. **A. Cell concentrations.** Cell concentrations were estimated using a Malassez counting chamber. **B. Chlorophyll content.** Spectrophotometric measurement of fluorescence was performed at 680 nm at room temperature using 10^6 cells.

External supply of NO• triggers the accumulation of triacylglycerol (TAG) within *P. tricornutum* cells

Cell division arrest following general stress responses is known to coincide with the accumulation of triacylglycerol (TAG) (Kohlwein, 2010; Meï et al., 2017). We analyzed the accumulation of TAG droplets in *Phaeodactylum* by Nile Red staining. Following exposure to NO•, we did not see any evidence of chloroplast disintegration or of cell death, as observed

following DD treatments. We observed that a 2-day incubation with 1 mM SNAP in a 500 µL culture volume triggered a 2.2 fold increase of TAG per cell (Figure 2A) and a >2 fold increase of TAG productivity, corresponding to the level of TAG per volume of culture and per day (Figure 2B). Interestingly, while upon nitrogen starvation two large lipid droplets are visible in *Phaeodactylum*, flanking the chloroplast (Abida et al., 2015), in SNAP treated cells numerous lipid droplets of variable sizes can be observed (Figure 2C).

Commented [WU1]: Where ? In the control (NAP-treated) cells ?

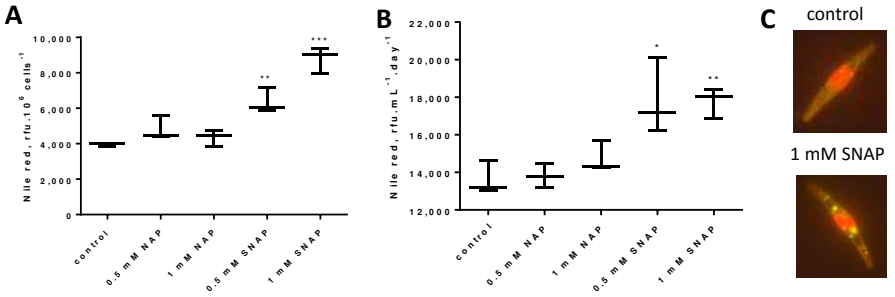

Figure 2. Effect of increasing concentrations of SNAP on the production of TAG in *Phaeodactylum tricornutum*. The incubation was performed in a volume of 500 µL, inoculated at 10^6 cells.mL^{-1}, with immediate addition of chemicals. Measurements were performed after 2 days of incubation. **A. Effect of increasing concentrations of SNAP on TAG level per cell.** TAG level per cell were measured using Nile Red staining and is given in relative fluorescence units per 10^6 cells. Stars indicate statistical relevant treated compared to untreated samples, with p-values of 5.10^{-3} and 4.10^{-4} for 0.5 mM SNAP and 1 mM SNAP, respectively. **B. Effect of increasing concentrations of SNAP on TAG productivity.** TAG productivity is given in relative fluorescence unit (Rfu) corresponding to the fluorescence of Nile Red per mL and per day. **(C) Epifluorescence images** on Nile red stained treated and untreated cells. Statistically relevant were the responses to 0.5 mM SNAP (p-value 3.10^{-2}) and 1 mM SNAP (p-value 4.10^{-4}).

We sought to determine whether this effect observed following an external supply of NO• could be also attributed to NO• as an internal signal, enzymatically produced by the diatom itself. To that purpose, we re-examined the question of the endogenous production of NO•.

Biosynthesis of NO• in *Phaeodactylum* is arginine-independent and nitrite-dependent.

Data from previous studies on NO• production by diatoms are confusing. On the one hand, it was shown that NO• production was blocked by an NOS-blocking agent (Vardi et al., 2006) and authors concluded on the action of a NOS-like enzyme using arginine as a substrate. Intriguingly, it was not possible to detect any NOS-like sequence in the genome of *P.*

tricornutum (Di Dato et al., 2015). On the other hand, an orthologous sequence of the plant chloroplast NO-associated (NOA) protein sequence was identified (Vardi et al., 2008). *NOA*-overexpression was reported to lead to a $NO^{\bullet}$ increase, a reduction of growth and a decrease of *Fv/Fm*. *NOA* overexpressing lines were also reported to be hypersensitive to DD, with a growth arrest at 3.3 µM or 6.6 µM DD, whereas WT cells were unaffected (Vardi et al., 2008), conditions that were shown here to trigger unspecific cell death in the WT.

The *Arabidopsis* homolog AtNOA acts in $NO^{\bullet}$ production but the protein does not possess any NOS function *in vitro* (Moreau et al., 2008). AtNOA1 and nitrate reductase (NR) are responsible for the majority of $NO^{\bullet}$ releases (Gas et al., 2009; Moreau et al., 2010). The mode of action of AtNOA1 remains elusive although it might be involved in the regulation of NR activity (Jin et al., 2009; Mandal et al., 2012). In this NR-dependent pathway, $NO^{\bullet}$ is produced by reduction of nitrite (NO_2^-) by NR (Figure S5). Nitrite is reduced to ammonium (NH_3) by the nitrite reductase (NIR), and ammonium is a substrate for the biosynthesis of arginine. Therefore, addition of arginine could have a negative feedback regulation on NIR thereby providing high nitrite levels for NR-dependent $NO^{\bullet}$ production (Figure S5). This could explain a positive action of an arginine supply on $NO^{\bullet}$ production, *via* NR and in the absence of any NOS. One way to make the distinction between $NO^{\bullet}$ produced from arginine *via* a NOS or *via* a NR is to detect an inhibition of the NOS-pathway by a blocking agent, *e.g.* L-NAME (Nω-nitro-L-arginine methyl ester).

We analyzed therefore the endogenous level of $NO^{\bullet}$ in *Phaeodactylum* culture in presence of the two potential substrates, arginine and NO_2^-. The detection of $NO^{\bullet}$ in *Phaeodactylum* was much higher when the diatoms were cultured in presence of NO_2^-, either in the presence or absence of NO_3^- (Figure 3), supporting a production *via* the action of NR. By contrast, addition of arginine did not impact significantly on the production of $NO^{\bullet}$. Similarly, addition of L-NAME did not lead to any significant change, when cells were co-fed with arginine (Figure 3).

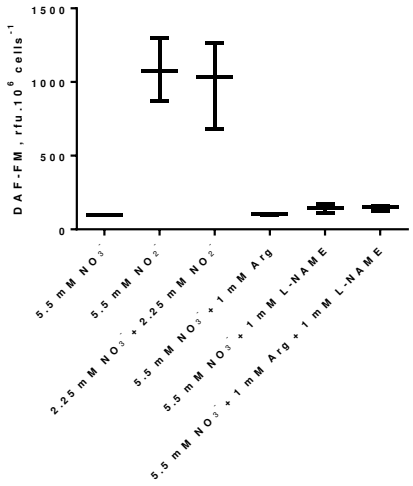

Figure 3. Detection of NO in *Phaedocatylum* based on nitrogen sources. Cells were harvested from complete media and inoculated in nitrogen-free media at 2.10^6 cells.mL^{-1}. DAF-FM was added at a concentration of 10 µM. After dark incubation and washing, cells were collected into 500 µL culture aliquots, and supplemented with the indicated nitrogen sources: nitrate (NO_3^-, standard medium), nitrite (NO_2^-), 1 mM arginine (Arg) and the NOS-blocking agent L-NAME. DAF-FM fluorescence was recorded after three hours of incubation.

Taken together, these results are consistent with a unique NR-dependent production of NO• in *Phaeodactylum* as observed in other photosynthetic eukaryotes from distant clades, such as *Arabidopsis* (Moreau et al., 2010; Sanz-Luque et al., 2015), the red alga *Gracilaria chilensis* (Chow et al., 2013) and the green alga *Chlamydomonas* (Wei et al., 2014). The previously reported NOS activity in *Phaeodactylum* (Vardi et al., 2006; Vardi et al., 2008) was based on increased NO• production in response to DD measured with a citrulline/arginine feeding on whole cell protein extracts (Vardi et al., 2006). Given the destructive effect of DD, one cannot exclude an interference with this method. In addition, we used the *Phaeodactylum* accession Pt1 CCAP 1055, whereas the previously study used CCMP 632, thus we cannot exclude strain-dependent differences.

NOA overexpression correlates with an increased endogenous production of NO• by *Phaeodactylum*

We re-examined the role of the NOA protein in the endogenous production of NO• and designed genetic constructions for *NOA* overexpression. Genomic DNA extracted from *P. tricornutum*

Pt1 strain was used as matrix and a 2,352 bp sequence was amplified by PCR using oligonucleotides designed from Phatr2_56150 (Vardi et al., 2008), now referenced as Phatr3_J40200. The *NOA* PCR product was cloned into the pH4 vector (De Riso et al., 2009), transformed into *P. tricornutum* WT cells and we obtained overexpressing lines after zeocin selection, including NOAOE4 and NOAOEf generated by two independent series of transformation experiments. The RNA level of the *NOA* gene was more than 30-fold induced in the two independent overexpressing lines and led to a 4-5-fold elevated $NO^{\bullet}$ production (Figure S6), which was consistent with previous reports (Vardi et al., 2008). We thus confirmed that NOA played a role in $NO^{\bullet}$ production and used these overexpressing lines as models for the analysis of the physiological role of $NO^{\bullet}$ in *Phaeodactylum*. We obtained similar results with both independent overexpressing lines and present below results obtained with NOAOE4.

NOA overexpression activates the transcription of the plastid ferredoxin-nitrite reductase.

In plants, the precise molecular function of NOA is unresolved, but some reports suggest an interplay with nitrogen assimilation (Yamasaki and Sakihama, 2000; Moreau et al., 2010). $NO^{\bullet}$ production was also correlated with a transcriptional control of nitrogen-assimilation genes, as described for *Chlamydomonas* (de Montaigu et al., 2010). We sought whether such transcriptional control could exist in *Phaeodactylum*. We analyzed by qRT-PCR the expression level of the genes coding for the cytosolic NR (Phatr3_J54983), the plastid ferredoxin-dependent nitrite reductase, NIR (Phatr3_J12902) and the sulfite reductase, SIR (Phatr3_J9538), used as a nitrogen-independent negative control. In nutrient replete conditions (10 x ESAW), the *NIR* gene was highly induced in NOAOE4, whereas *NR* expression was slightly increased and that of *SIR* did not change significantly, compared to the respective wild type and cells transformed with the empty vector (Figure 4A). A nitrite-sensing module can therefore be proposed based on a positive regulatory loop triggering *NIR* transcription downstream NR-dependent transient $NO^{\bullet}$ emission (Figure 4B).

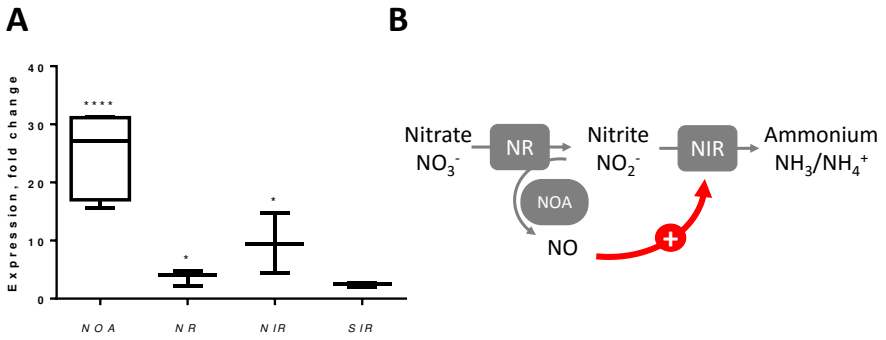

Figure 4: Effect of NOA overexpression on the expression level of nitrogen assimilation genes in nutrient replete condition. A. NOA overexpression activates the transcription of the plastid ferredoxin-nitrite reductase. RNA was extracted from a 10^8-cell pellet of NOAOE4, WT and pH4 and reversely transcribed. Quantitative real time PCR was conducted on 20 ng cDNA using oligonucleotides binding *TUB* and *RPS* as internal controls and *NOA, NR, NIR* and *SIR* as genes of interest. Quantification cycles of NOAOE4 derived cDNA were normalized to WT and pH4 values. Significant changes were observed on the level of *NOA* (p-value < 10^{-4}), *NR* (p-value $1.25.10^{-2}$) and *NIR* (p-value 2.10^{-2}). **B. Nitrite-sensing module.** Abbreviations: NIR, plastid ferredoxin-dependent nitrite reductase; NOA, plastid nitric oxide associated protein; NR, cytosolic nitrate reductase; SIR, sulfite reductase.

NOA does not appear involved in the onset of the response of *Phaeodactylum* to nitrogen starvation.

Since *Phaeodactylum* increases *NR* expression levels when nitrogen is limited (Levitan et al., 2015; Yang et al., 2016), and since *NR* expression was slightly increased in the NOAOE background, we sought to determine whether NOA was also responsive to nitrogen availability. In a 3-day time course of cells shifted to nitrogen depleted conditions, the typical nitrogen starvation responses occurred, *i.e.* reduction of *Fv*/*Fm*, chlorophyll fluorescence and cell growth and induction of neutral lipids as measured by Nile Red staining (Figure 5A). We confirmed a rapid, strong and parallel induction of *NR* and *NIR* in response to nitrogen starvation (Figure 5B). *SIR* and *NOA* responded to general nutrient deprivation with a late induction pattern, reaching a maximal 4-6-fold induction after three days of cultivation (Figure 5B). Thus, although in nutrient-replete culture we had observed the overexpression of *NOA* with higher *NR* and *NIR* levels, under nitrogen starvation the upregulation of these genes is not synchronized downstream an increase of *NOA* mRNA. This is in contrast with *Chlamydomonas*,

in which NO• was shown to be produced from cytosolic nitrite, and act in the orchestrated response upon nitrogen shortage (Miller et al., 2010; Wei et al., 2014). In *Phaeodactylum*, NO• does not appear as a mediator in the onset of the phosphate deprivation response.

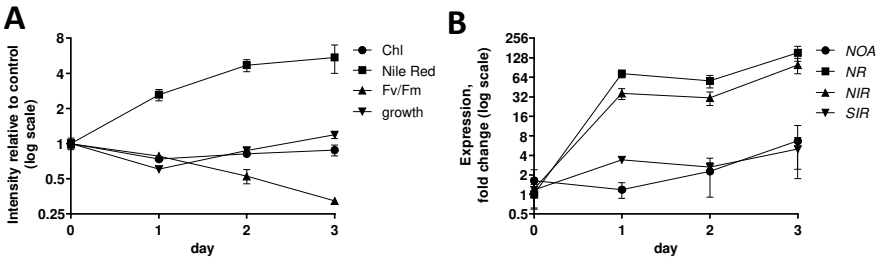

Figure 5: Expression of *NOA*, *NR*, *NIR* and *SIR* in nitrogen depleted wild-type *Phaeodactylum* cells . Cells were harvested and resuspended in nitrogen-free media in 100 mL cultures a concentration of 10^6 cells.mL^{-1}. Each day, a 20 mL culture aliquot was harvested for RNA extraction and a 300-µL culture aliquot was used for physiological measurements. **A. Physiological parameters.** Chlorophyll (Chl) was measured by the absorption at 680 nm at room temperature, Nile red fluorescence was quantified to indicate neutral lipid contents, *Fv/Fm* was measured using fast chlorophyll fluorescence kinetics and cell concentrations were estimated via the absorption at 750 nm. **B. *NOA*, *NR*, *NIR* and *SIR* gene expression.** RNA was extracted from a cell pellet and reversely transcribed. Quantitative real time PCR was conducted on 20 ng cDNA using oligonucleotides binding *TUB* and *RPS* as internal controls and *NOA, NR* and *NIR* as genes of interest. The *SIR* gene was used as a nitrogen-unrelated control. Data are normalized with value measured with cells harvested before the shift. Data are the results of three independent biological replicates.

Altogether, these results support a role of NOA and NO• in a fine tuning of the regulation of the nitrogen assimilation system more selective for nitrite over nitrate (uncoupled and higher upregulation of *NIR* over *NR*), but this NO•-mediated pathway does not operate during nitrogen starvation, where a strong and parallel up-regulation of *NR* and *NIR* is triggered. We sought to characterize the extent of the transcriptional changes induces by NO• at the whole genome scale.

Whole genome transcriptome analysis in response to increasing doses of NO• highlights a role in nitrite sensing, high-nitrite adaptation and reprogramming of lipid synthesis.

We analyzed the effects of increasing doses of NO• on the whole transcriptome of *Phaeodactylum*. To that purpose, we supplied NO• from a saturated solution at concentrations of 3 and 10 µM. Of the 12,393 referenced genes, reads were obtained for 11,464 . We found 804 genes differentially expressed with a |Log2(fold change)| > 1 in at least one of the contrasts (i.e. comparing NO• supplies at 0 µM vs. 3 µM, 0 µM vs. 10 µM or 3 µM vs. 10 µM), and with p-value lower than 0.05. A partition of differentially expressed genes was performed using a *K*-

mean method, with the number of partitions set to 6 (Liu et al., 2014). Each group or cluster consisted of genes with similarexpression profiles following treatments with $NO^{\bullet}$ (Figure S7 and Table S1). Two clusters were comprised of genes downregulated following $NO^{\bullet}$ treatments, *i.e.* group 1 (DR_1; 55 genes) containing genes with the strongest magnitude in decreased expression (in the -2 to -4 Log2FC range) and group 2 (DR_2; 282 genes) with moderate but significant decreased expression (Log2FC ~ -1). Likewise, two clusters were comprised of genes upregulated following $NO^{\bullet}$ treatments, *i.e.* group 6 (UR_1; 54 genes) containing genes with the strongest magnitude in expression increase (in the +2 to +4 Log2FC range) and group 3 (UR_2; 291 genes) with moderate but significant increased expression (Log2FC ~ +1) (Figure S7 and Table S1). For each group we sought whether gene ontology (GO) terms could be enriched, either by the DAVID method (http://david.abcc.ncifcrf.gov) (Huang et al., 2007) (Table S2) or using the GOseq R package (Young et al., 2010) (Table S3). We then mined information in the groups corresponding to a differential expression that could be correlated with the dose, *i.e.* DR_1, DR_2, UR_1 and UR_2.

Focusing on genes apparently upregulated by $NO^{\bullet}$, we focused on the possible metabolic pathways or cellular processes responsible for this reprogramming. Clearly, GO terms and metabolic pathways corresponding to nitrogen assimilation, glycolysis, phosphoenolpyruvate production, pyruvate production, acetyl-CoA production and glycerolipid production are enriched in UR_1 and UR_2 (in bold characters and underlined in Tables S2 and S3). More specific GO terms retrieved concerning nitrogen metabolism include the carbamoyl synthase activity, arginosuccinate synthetase activity, glutamine synthesis and arginine synthesis. These terms highlight a possible activation of two pathways generating amino acids, *i.e.* the glutamine synthase/glutamine oxoglutarate aminotransferase ("GS/GOGAT") route producing glutamine and glutamate, and the ornithine-urea pathway. More specific GO terms retrieved concerning carbon metabolism include glycolysis, phosphopyruvate hydratase activity, phosphoglycerate kinase activity and lipid metabolism.

We thus focused our analysis on the corresponding metabolic pathways. Figure 6A shows the dose-dependent response of genes involved in nitrogen (nitrate, nitrite, ammonium) assimilation, incorporation into amino acids and entry into the ornithine-urea pathway, which was shown to be a specific metabolic feature of diatoms (reference?). The most evident response to low-dose treatments with $NO^{\bullet}$ amongst the set of genes known to be involved in nitrogen assimilation is the specific expression of the gene coding for the plastid NIR protein, reducing NO_2^- into NH_3/NH_4^+ (Figure 6A). We included in this analysis the gene putatively

coding for the large subunit of a prokaryotic-type NADPH dependent nitrite reductase (*NASB*) (Allen et al., 2011; Levitan et al., 2015), and is clearly uncoupled from the high-nitrite adaptive response shown here (Figure 6A) Genes coding for enzymes involved in nitrogen incorporation into amino acids *via* the "GS/GOGAT" route (Guerra et al., 2013), are upregulated starting with the incorporation of NH_3 into glutamine by GLNA, followed by the production of glutamate by the glutamate synthase systems, Mito-GLTX, Plastid-GLT and GLTD. This upregulated pathway is localized in the plastid, where NIR also resides (Figure 6).

Genes encoding the ornithine-urea pathway are clearly and coordinately activated, to the notable exception of one of its components, the arginase gene, *ARG* (Figure 6A). Firstly, the mitochondrial carbamoyl phosphate synthase, CPS III, combining CO_2 and NH_4^+ into carbamoyl phosphate, is upregulated. Following this capture of ammonium, carbamoyl phosphate is combined with ornithine by the OTC, forming citrulline, then combined with aspartate by the argininosuccinate synthase, ASUS. Argininosuccinate is broken down into arginine and fumarate by the argininosuccinate lyase, ASL. Whereas *CPS III*, *OTC*, *ASUS* and *ASL* are all activated, *ARG* encoding the enzyme regenerating ornithine and producing urea is unchanged, even slightly downregulated. The so-called ornithine-urea cycle is therefore not cyclic, interrupted at the level of arginine (Figure 6B) and it appears therefore as a system mainly tuned to capture NH_4^+, without driving the production of urea. Consistently, the gene encoding the urease, *URE*, is also activated in parallel with the others, breaking down urea back into NH_4^+ and CO_2. Ornithine, which needs to be recycled to allow this pathway to operate, can alternatively derive from glutamate and acetyl-CoA, produced by an acetylornithine deacetylase. Two proteins containing zinc-peptidase like domains in *Phaeodactylum* (Phatr3_J15083 and Phatr3_J18404) might possibly produce ornithine by this pathway, but this function needs to be demonstrated. Taken together, all genes of the ornithine-urea pathway seem to be mobilized to trap ammonium produced by NIR and use it to produce arginine.

Interestingly, exogenous $NO^\bullet$ does not trigger the upregulation of *NOA* (Figure 6A). We sought sequences in the genome of *Phaeodactylum* which might be homologous to genes involved in $NO^\bullet$ signaling in other eukaryotes. As mentioned above, no *NOS* gene could be identified (Di Dato et al., 2015). Genes coding for homologues of a NOS-interacting protein and an NADPH-cytochrome P450 NOS homologue have been found, but their annotation is likely not valid, and they do not respond to the $NO^\bullet$ treatment (Figure 6A). Thus our analysis could not lead us to identify any component acting in the synthesis of $NO^\bullet$ besides NOA.

Note: The column headings in this Figure should be changed to 3 and 10 µM instead of 30 and 60 µM.

A

		gene name	gene ID	Log2(30µM NO/Control)	Log2(60µM NO/Control)
Nitrogen assimilation	Nitrate transporter	NIT1	Phatr3_J26029		
	Nitrate reductase	NR	Phatr3_J54983		
	Nitrite transporter, plastid	NAR1	Phatr3_J13076		
	Ferredoxin nitrite reductase, plastid	NIR	Phatr3_J12902		
	Putative NADPH nitrite reductase, plastid	NASB	Phatr3_EG02286		
Sulfite reduction	Ferredoxin sulfite reductase, plastid	SIR	Phatr3_J9538		
Integration of N into amino acids	Ferredoxin-dependent glutamate synthase, fusion of large and small subunits, GOGAT	Mito-GLTX	Phatr3_J51214		
	Synthase of glutamate synthase, GOGAT	GLTD	Phatr3_J20342		
	Glutamate synthase, fusion of large and small subunits, GOGAT	Plastid-GLT	Phatr3_J24739		
	Glutamine synthase, GS	GLNA	Phatr3_J22357		
Ornithine-Urea Cycle	Ammonium-dependent carbamoyl-phosphate synthase, mitochondrial	CPS III	Phatr3_J24195		
	Ornithine transcarbamylase, mitochondrial	OTC	Phatr3_J30514		
	Argininosuccinate synthetase	ASUS	Phatr3_J21116		
	Argininosuccinate lyase	ASL	Phatr3_J34526		
	Arginase	ARG	Phatr3_J38509		
	Ornithine decarboxylase	ODC	Phatr3_J12642		
	Ornithine cyclodeaminase/proline synthase	OCD	Phatr3_J54222		
	Urease	URE	Phatr3_J29702		
	Agmatinase/polyamine synthase	AGM	Phatr3_J40880		
Cytosolic carbamoylation (pyrimidine synthesis)	Glutamine-hydrolyzing carbamoyl-phosphate synthase, cytosolic	CPS II	Phatr3_EG01947		
Nitric oxide signalling	Nitric oxide associated protein, plastid	NOA	Phatr3_J40200		
	Homologue of a Nitric oxide synthase-interacting protein (E3 Ligase)	-	Phatr3_J46175		
	Cytosolic Nucleic Acid Binding Protein	NAB1-Like	Phatr3_J15211		
	NADPH-cytochrome P450 reductase, NOS and SiR homologue	PCR	Phatr3_J45758		

Color code	LogFC range
	< -0.9
	-0.9 to -0.5
	-0.5 to -0.25
	-0.25 to 0.0
	0.0 to 0.25
	0.25 to 0.5
	0.5 to 0.9
	> 0.9

B

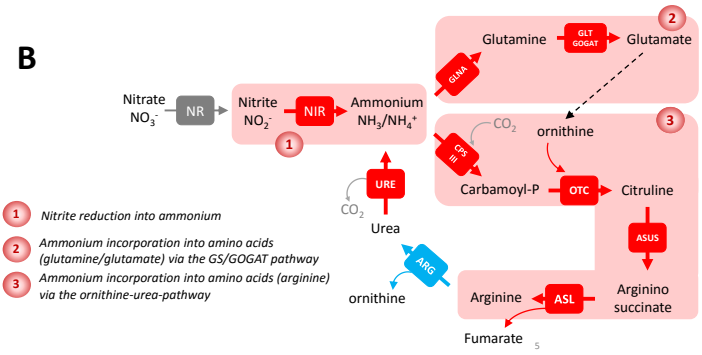

Figure 6: Dose-response expression of nitrogen assimilation genes following treatment with increasing concentrations of NO•. *Phaeodactylum* cells were treated with 0 (Control), 3 µM and 10 µM NO• using a calibrated NO•-saturated aqueous solution and after 96 hours of NO• treatment, RNA was extracted and subjected to a RNAseq aalysis. Libraries for each sample were prepared for stranded 100 bp paired end sequencing and samples were combined and analyzed in a single Illumina Hiseq 2000 lane. Reads were mapped on the most recent genome version of *Phaeodactylum tricornutum* (http://protists.ensembl.org/Phaeodactylum_tricornutum). Annotated genes coding for nitrogen assimilation were then used to probe changes in 3 metabolic modules, *i.e.* nitrogen assimilation, integration of nitrogen into amino acids and integration of nitrogen *via* the ornithine-urea pathway (or cycle). *NOA* expression was also examined. Eventually, genes with some sequence similarity with genes acting in NO• signaling in other organisms were also included, although this function seems unlikely based on our study.

Recently, NO• has been shown to nitrosylate a RNA-binding protein in the cytosol of *Chlamydomonas*, NAB1, which represses the translation of some mRNAs of photosynthetic

components such as LHC II isoforms (Berger et al., 2016). A NAB1-like sequence was identified, lacking the nitrosylated domain identified in the *Chlamydomonas* sequence; nevertheless, the *NAB1-like* gene appeared as upregulated by the treatment.

In this reprogramming, the $NO_2^- \rightarrow NH_3/NH_4^+ \rightarrow$ amino acid route is uncoupled from nitrate assimilation, and activates both the GS/GOGAT and the ornithine-urea pathway as the two gates to incorporate NH_3/NH_4^+ (Figure 6B). The GS/GOGAT route alone was reported previously to be a key regulatory site for the nitrate-dependent control of carbon partitioning between protein and lipid biosynthesis (Guerra et al., 2013). Lipid should therefore not accumulate. By contrast, the *ARG* gene being uncoupled from the general upregulation of the ornithine-urea pathway, fumarate is expected to accumulate and feed carbon metabolism *via* malate. Based on the GO enrichment analysis, the phosphoenolpyruvate/pyruvate (PEP/Pyr) hub and acyl-lipid metabolism were highlighted in differentially expressed genes. We thus examined the acyl-lipid anabolism and catabolism in more details, using a table of genes annotated for this purpose (Table S4).

The most striking feature in carbon metabolism reprogramming is the coordinated upregulation of the pathway synthesizing PEP, Pyr and acetyl-CoA in the plastid (Table S4). These include the gene coding for the plastid glyceraldehyde-3-phosphate dehydrogenase, *Plastid-GAP* (Phatr3_J22122), the phosphoglycerate kinase, *Plastid-PGK* (Phatr3_J29157) and the enolase, *Plastid-ENOL* (Phatr3_J41515), leading to the synthesis of PEP. The pyruvate kinase, *Plastid-PKP* (Phatr3_J22404), leading to the production of Pyr, and two genes coding for dihydrolipoamide acetyltransferase E2 components of the pyruvate dehydrogenase complex, *Plastid-DHLATa* and *Plastid-DHLATb* (Phatr3_J23850 and Phatr3_EG02309) are upregulated, acting in the direction of a production of acetyl-CoA (Table S4). Based on this transcriptome reprogramming, carbon metabolism, including the excess of fumarate generated by the activated ornithine-urea cycle, can converge toward a production of acetyl-CoA.

Downstream of acetyl-CoA, the feeding of fatty acid and TAG biosynthesis is not obvious based on the transcriptomic response to $NO^{\bullet}$. Only one component of the fatty acid synthase of type II (FASII) appears upregulated, *i.e.* a ketoacyl-ACP synthase, *Plastid-KASb* (Phatr3_J52648) (Table S4). Then the production of a diacyl moiety in the plastid appears slightly stimulated *via* a coordinated upregulation of a glycerol-3-phosphate acyltransferase, *ATS1* (Phatr3_J3262) and two 1-acylglycerol-3-phosphate acyltransferases, *ATS2a* and *ATS2b* (Phatr3_J11916 and Phatr3_J43099). The production of TAG could be sustained by a moderate upregulation of an ER localized acyl-CoA:diacylglycerol acyltransferase, *DGAT2B*

(Phatr3_J49544). Genes coding for enzymes involved in TAG and fatty acid degradation do not respond significantly to the NO• treatment (Table S4).

The gene coding for the lipid droplet protein, *LDP* (Phatr3_J48859) (Yoneda et al., 2016) is upregulated as an unambiguous marker of TAG accumulation. In addition, two lipases that could possibly degrade TAG are downregulated, *i.e.* a TAG lipase gene, *TAGL-Like-B* (Phatr3_J48799 and a phospholipase A, *PLA-A* (Phatr3_J44005) (Table S4). An accumulation of TAG can therefore occur *via* a "push"/ "protect" activated process, "pushing" at the level of acetyl-CoA production and to some extent fatty acid synthesis and "protecting" by producing LDP and preventing TAG-hydrolysis.

An intriguing coordinated response was the upregulation of fatty acid (FA) desaturase genes (Dolch and Marechal, 2015): the plastid ω6-acyl-lipid desaturase, *FAD6* (Phatr3_J48423), the plastid Δ6-FA desaturase, *Plastid-Delta6FAD* (Phatr3_EG02619), the ER localized ω6-acyl-lipid desaturase, *FAD2* (Phatr3_J25769), an ER localized Δ5-FA front-end desaturase, *ER-delta5-FAD-A* (Phatr3_J46830) and Δ6-FA front-end desaturase, *ER-delta6-FAD* (Phatr3_J29488) (Table S4). This indicates a general activation of FA desaturation, which could compensate polyunsaturated FA nitrated *via* NO•-derived radicals, forming NO_2-FAs (Baker et al., 2009; Sanchez-Calvo et al., 2013; Fazzari et al., 2014). One should therefore expect that such upregulation of FA desaturase genes follows a drop in polyunsaturated fatty acids.

Taken together, the remodeling of lipid upon exposure to NO• seems not solely based on gene expression reprogramming, since only TAG accumulation could possibly be activated transcriptionally, whereas a compensating mechanism for a loss of very-long chain polyunsaturated fatty acids seems to be activated. We sought therefore to refine our analysis of lipid changes and advance in the possible mechanism of action of NO• in this remodeling.

NOA induces a specific glycerolipid remodeling in *Phaeodactylum*, marked by a change in the MGDG/TAG balance.

Comprehensive lipid analyses need cell amounts that could not be obtained with the treatment of WT cells with NO•. Using NOAOE lines as a model of a non-transient exposure to NO•, we could observe that in nutrient replete conditions, the level of TAG per cell estimated by Nile Red staining was higher, consistent with a larger number of intracellular lipid droplets, as observed for SNAP treated cells (Figure S8). We extracted lipids and performed fatty acid analyses and whole glycerolipidomic profiling. Consistent with the Nile Red measurements, the total fatty acid profile of NOAOE lines compared to the WT indicated significantly higher

16:0 and 18:0 levels and a 2.3 fold increase in TAG productivity (Figure 7A and C). By contrast, very long chain polyunsaturated fatty acids (VLC-PUFAs) displayed trends of reductions and accordingly the greatest sink for VLC-PUFAs, *i.e.* chloroplast monogalactosyldiacylglycerol (MGDG), was significantly reduced in the overexpression lines (Figure 7B). The distribution of fatty acids in the different lipid classes was reported previously (Abida et al., 2015) and was similar in the present study. The fatty acid profiles in TAG and MGDG lipid classes were unaltered (Figure S9)

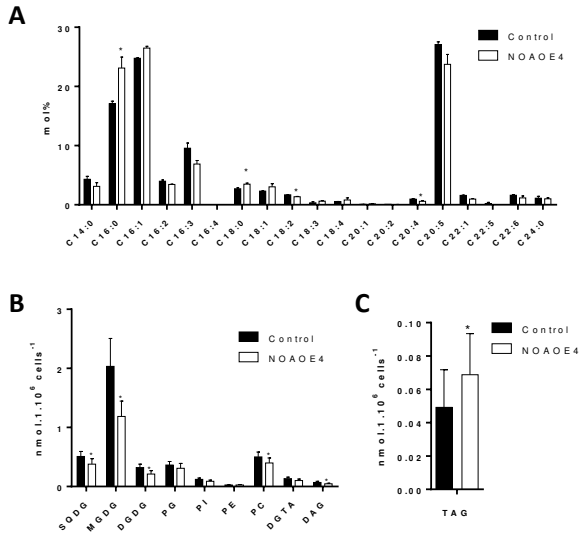

Figure 7: Effect of NOA overexpression on total fatty acid and glycerolipid profiles in *Phaeodactylum* cells grown in nutrient replete conditions. Three day old 50 mL cultures inoculated at 10^6 cells ml^{-1} were harvested and lipids extracted. **A. Total fatty acid distributions.** The fatty acid distribution in total lipid extracts was based on GC-FID analyses of fatty acid methyl esters. **B. Membrane glycerolipid profiles. C. Triacylglycerol content.** Glycerolipid class abundances per million cells were assessed based on HPLC-MS/MS analyses, as described previously (Abida et al., 2015). Data are the result of triplicate analyses. DAG, diacylglycerol; DGDG, digalactosyldiacylglycerol; DGTA, diacylglyceryl hydroxymethyltrimethyl-β-alanine, MGDG, monogalactosyldiacylglycerol; PC, phosphatidylcholine; PE, phosphatidylethanolamine; PG, phosphatidylglycerol; PI, phosphatidylinositide; SQDG, sulfoquinovosyldiacylglycerol; TAG, triacylglycerol. Stars indicate significant changes with p-values < 0.05.

According to the lipid profiles, only the abundance of MGDG and TAG were affected in NOAOE lines compared to the WT. The increase in TAG is consistent with the transcriptomic analyses reported above, as evidenced by the coordinated upregulation of genes involved in

acetyl-CoA production, TAG biosynthesis, and the gene coding for the lipid droplet protein, LDP. Among the putative genes possibly involved in MGDG biosynthesis, *MGD1*, *MGD2* and *MGD3* (Phatr3_J54168, Phatr3_J9619, Phatr3_J14125), no read could be counted for *MGD3* and the expression of *MGD1* and *MGD2* was not significantly altered upon NO• treatment (Table S4). We sought to determine whether the decrease in galactolipids could occur by a direct effect of NO• on MGD activity.

Direct inhibitory effect of NO• on the enzymatic activity of *Phaeodactylum* MGDG synthase

We used the enzymatic assay developed for plant MGDG synthase, providing radioactive UDP-galactose to *Phaeodactylum* protein extracts, and measured the incorporation of the radioactivity in galactolipids extracted by solvents, following incubation with increasing concentrations of SNAP (Figure 8A). MGDG synthase activity was altered, with a 50% decrease following incubation with 0.5 mM SNAP. This result showed that NO• can affect MGDG synthases, likely by S-nitrosylation of the thiol groups known to be essential for the activity of this enzyme (Marechal et al., 1994; Marechal et al., 1995). This enzymatic inhibition could be responsible for a decrease of plastid glycerolipid biosynthesis, and thus contribute to the partial redirection of glycerolipid flux toward TAG (Figure 8B).

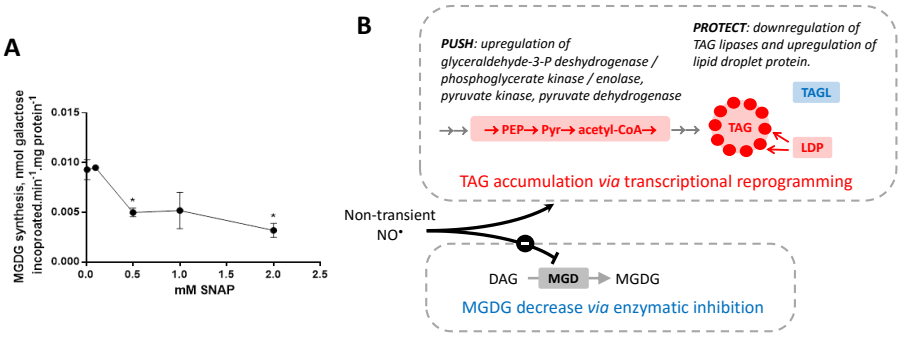

Figure 8: A. Effect of NO• on the MGDG synthase activity in *Phaeodactylum* membrane extracts. Activity was assayed based on the incorporation of galactose in MGDG, following incubation with radiolabeled UDP-[^{14}C]galactose. Data are the results of three technical replicates. Stars indicate significant changes with p-values < 0.05. **B. Lipid remodeling *via* transcriptional reprogramming and enzymatic regulation.**

Taken together, the lipid remodeling occurring in *Phaeodactylum* requires the combination of a transcriptome reprogramming with a post-translational control of some enzymes. On the one hand, a coordinated transcriptomic reprogramming converges on acetyl-CoA production, which could thus integrate fumarate, a side-product of NH_3/NH_4^+ integration *via* the ornithine-urea

pathway. Acetyl-CoA can feed fatty acid biosynthesis and, *via* the upregulation of some genes involved in TAG biosynthesis and most importantly the LDP protecting the lipid droplet, the accumulation of oil. On the other hand, the biosynthesis of MGDG particularly enriched in VLC-PUFAs, known to be susceptible to NO•, is down-regulated post-translationally (Figure 8B). The loss of VLC-PUFAs is partly compensated for by the coordinated upregulation of desaturase genes (Table S4).

Biotechnological perspectives: the impact of NO• in diatom cultivation and the development of strains overexpressing *NOA*

The study presented here illustrates that a supply of NO• in a cultivation medium could have both deleterious (growth retardation) and beneficial (TAG accumulation) effects on such diatoms as *Phaeodactylum* for industrial purposes. These two opposite effects being balanced in terms of TAG productivity, NO• might therefore be considered as an interesting component in flue gases or waste waters for industrial cultivation for oil production. One should keep in mind that not all diatoms lack a *NOS* gene (Di Dato et al., 2015) and that the remodeling of carbon metabolism reported here seems to depend, at least partly, on the presence of the ornithine-urea pathway, producing fumarate as a side-product. The supplementation with NO_2^- is not expected to have an effect with the same magnitude, since the endogenous production of NO• it induces acts on a better incorporation of nitrite and therefore on a decline of NO• (the role of NO• in nitrite sensing is transient). Exogenous addition of NO• can be considered as a way to trigger TAG accumulation, being effective on TAG productivity. The TAG increase in *NOA*-overexpressing lines, even moderate, could also be interesting for oil production in diatoms grown in nutrient replete conditions. We evaluated this increase in a pilot experiment, with a supply of air or 1.5% CO_2 and in two growth media, using a multicutivator system consisting of air-lift photobioreactors run in parallel. This comparison was performed between WT and NOAOE4 grown in 50 ml of medium ESAW or medium F for 8 days (late exponential growth phase). Illumination was set to 60 µE m^{-2} s^{-1} for the first three days of cultivation and then increased to 120 µE m^{-2} s^{-1} on day 4 until samples were collected at day 8. Lipids were analyzed from collected cells by LC-MSMS. The supply of CO_2 and the modification of media had no impact on the phenotype due to NOA overexpression, with WT *Phaeodactylum* accumulating 21-45 µg TAG per 10^6 cells (50-101 µg mL^{-1}) and NOAOE4 accumulating 101-119 µg TAG per 10^6 cells (105-145 µg mL^{-1}). Altogether, our comparisons show that NOA overexpression leads to a doubling in TAG content and productivity in *Phaeodactylum* grown in non-limiting CO_2 conditions.

Conclusion.

In summary, this study was motivated by evaluating the possible impact of environmental variations of the NO• level in oceans on phytoplankton, and more particularly diatoms. NO• was previously reported to be emitted by diatoms in response to high concentrations of PUAs and then to act in cell-to-cell communication, triggering PCD and allowing diatom population size control (Vardi et al., 2006; Vardi, 2008; Vardi et al., 2008; Bidle, 2015). Using *Phaeodactylum* as a model, we could not confirm the physiological response to DD applied at micromolar doses, that is supposed to trigger a specific production of NO•. DD appeared highly cytotoxic, as well as the cPTIO scavenger of NO•, previously reported to act as an antidote of the DD effect. Likewise, we could not confirm the previously reported production of NO• by a NOS-like activity using arginine as a substrate, and could not inhibit the NO• production by a NOS inhibitor (Vardi et al., 2006; Vardi et al., 2008). Rather, our work shows that in *Phaeodactylum* wild type cells, NO• is produced *via* a nitrate-dependent pathway, by a side activity of the NR. The nitrite-sensing role of NO• is very likely transient, since the assimilation of nitrite and its reduced form, ammonium, is coordinately upregulated at transcriptional level, activating both amino acid biosynthesis and the ornithine-urea pathway.

A non-transient exogenous supply of NO• inhibits growth. We sought whether a role in stress signaling could be detected. We confirmed that the overexpression of *NOA* was correlated with an increase in endogenous NO• (Vardi et al., 2008), but could not provide any evidence on the way NOA controls this level. Our analyses are consistent with a role of NO• on the remodeling of glycerolipids redirecting the flux toward the production of TAG, at least partly *via* transcriptomic reprogramming, and the specific decrease of MGDG, by enzymatic inhibition of MGD activity. A role of NO• in mediating PCD could not be observed.

The triggering of TAG accumulation by NO• is also interesting for biotechnological applications aiming at using diatoms for producing oil as a feedstock. We observed the phenotype of *NOA*-overexpressing lines, with a doubling of TAG content per cell and an increase in overall productivity in both flasks and photobioreactor systems, with different growth media and with or without CO_2 supply. Part of the carbon requested for the production of TAG is likely to derive from fumarate, a side product of the ornithine-urea pathway, which is one of the two entry gates to incorporate NH_3/NH_4^+. This specific feature of diatoms is consistent with previous studies showing that lipid production in *P. tricornutum* could be optimized when nitrate assimilation was inhibited and ammonium was the sole nitrogen source (Frada et al., 2013).

In conclusion, we propose a revision of the physiological and ecophysiological role of NO• in diatoms, primarily related to the environmental nitrogen status. An increase of NO• in the environment could therefore act as an important stressor at the ecosystem level. Future works include therefore the characterization of the interplay between nitrate, nitrite and nitric oxide in diatoms, involving *NR*, *NIR,* amino acid biosynthesis, ornithine-urea pathway and *NOA*, the functional characterization of these genes and then a re-evaluation of a possible role of NO• in the response to abiotic or biotic stresses.

Acknowledgements

This work was supported by grants from Agence Nationale de la Recherche (ANR DiaDomOil), CEA (Irtelis PhD grant program), the CEA-Total partnership, Programme Investissement d'Avenir (Océanomics) and from the National Research Council of Canada's Algal Carbon Conversion Program. The authors wish to thank Colleen Murphy for conducting the RNA extractions used for the RNASeq experiments.

References

Abida H, Dolch LJ, Mei C, Villanova V, Conte M, Block MA, Finazzi G, Bastien O, Tirichine L, Bowler C, Rebeille F, Petroutsos D, Jouhet J, Marechal E (2015) Membrane glycerolipid remodeling triggered by nitrogen and phosphorus starvation in Phaeodactylum tricornutum. Plant Physiol **167:** 118-136

Allen AE, Dupont CL, Obornik M, Horak A, Nunes-Nesi A, McCrow JP, Zheng H, Johnson DA, Hu H, Fernie AR, Bowler C (2011) Evolution and metabolic significance of the urea cycle in photosynthetic diatoms. Nature **473:** 203-207

Allorent G, Courtois F, Chevalier F, Lerbs-Mache S (2013) Plastid gene expression during chloroplast differentiation and dedifferentiation into non-photosynthetic plastids during seed formation. Plant Mol Biol **82:** 59-70

Baker PR, Schopfer FJ, O'Donnell VB, Freeman BA (2009) Convergence of nitric oxide and lipid signaling: anti-inflammatory nitro-fatty acids. Free Radic Biol Med **46:** 989-1003

Benvenuti G, Bosma R, Cuaresma M, Janssen M, Barbosa MJ, Wijffels RH (2015) Selecting microalgae with high lipid productivity and photosynthetic activity under nitrogen starvation. Journal of Applied Phycology **27:** 1425-1431

Berger H, De Mia M, Morisse S, Marchand CH, Lemaire SD, Wobbe L, Kruse O (2016) A Light Switch Based on Protein S-Nitrosylation Fine-Tunes Photosynthetic Light Harvesting in Chlamydomonas. Plant Physiol **171:** 821-832

Bidle KD (2015) The molecular ecophysiology of programmed cell death in marine phytoplankton. Ann Rev Mar Sci **7:** 341-375

Bligh GE, Dyer WJ (1959) A rapid method of total lipid extraction and purification. Can. J. Biochem. Physiol. **37:** 911-917

Casotti R, Mazza S, Brunet C, Vantrepotte V, Ianora A, Miralto A (2005) Growth inhibition and toxicity of the diatom aldehyde 2-trans, 4-trans-decadienal on Thalassiosira weissflogii (Bacillariophyceae). Journal of Phycology **41:** 7-20

Chow F, Pedersen M, Oliveira MC (2013) Modulation of nitrate reductase activity by photosynthetic electron transport chain and nitric oxide balance in the red macroalga Gracilaria chilensis (Gracilariales, Rhodophyta). Journal of Applied Phycology **25:** 1847-1853

Cooksey KE, Guckert B, Williams SA, Callis PR (1987) Fluorometric determination of the neutral lipid content of microalgal cells using Nile Red. J. Microbiol. Meth. **6:** 333-345

de Montaigu A, Sanz-Luque E, Galvan A, Fernandez E (2010) A soluble guanylate cyclase mediates negative signaling by ammonium on expression of nitrate reductase in Chlamydomonas. Plant Cell **22:** 1532-1548

De Riso V, Raniello R, Maumus F, Rogato A, Bowler C, Falciatore A (2009) Gene silencing in the marine diatom Phaeodactylum tricornutum. Nucleic Acids Res **37:** e96

Di Dato V, Musacchia F, Petrosino G, Patil S, Montresor M, Sanges R, Ferrante MI (2015) Transcriptome sequencing of three Pseudo-nitzschia species reveals comparable gene sets and the presence of Nitric Oxide Synthase genes in diatoms. Sci Rep **5:** 12329

Dobin A, Davis CA, Schlesinger F, Drenkow J, Zaleski C, Jha S, Batut P, Chaisson M, Gingeras TR (2013) STAR: ultrafast universal RNA-seq aligner. Bioinformatics **29:** 15-21

Dolch LJ, Marechal E (2015) Inventory of fatty acid desaturases in the pennate diatom Phaeodactylum tricornutum. Mar Drugs **13:** 1317-1339

Engstrom PG, Steijger T, Sipos B, Grant GR, Kahles A, Ratsch G, Goldman N, Hubbard TJ, Harrow J, Guigo R, Bertone P, Consortium R (2013) Systematic evaluation of spliced alignment programs for RNA-seq data. Nat Methods **10:** 1185-1191

Eroglu E, Gottschalk B, Charoensin S, Blass S, Bischof H, Rost R, Madreiter-Sokolowski CT, Pelzmann B, Bernhart E, Sattler W, Hallstrom S, Malinski T, Waldeck-Weiermair M, Graier WF, Malli R (2016) Development of novel FP-based probes for live-cell imaging of nitric oxide dynamics. Nat Commun **7:** 10623

Falciatore A, Casotti R, Leblanc C, Abrescia C, Bowler C (1999) Transformation of Nonselectable Reporter Genes in Marine Diatoms. Mar Biotechnol (NY) **1:** 239-251

Falciatore A, d'Alcala MR, Croot P, Bowler C (2000) Perception of environmental signals by a marine diatom. Science **288:** 2363-2366

Fazzari M, Trostchansky A, Schopfer FJ, Salvatore SR, Sanchez-Calvo B, Vitturi D, Valderrama R, Barroso JB, Radi R, Freeman BA, Rubbo H (2014) Olives and olive oil are sources of electrophilic fatty acid nitroalkenes. PLoS One **9:** e84884

Fowler D, Coyle M, Skiba U, Sutton MA, Cape JN, Reis S, Sheppard LJ, Jenkins A, Grizzetti B, Galloway JN, Vitousek P, Leach A, Bouwman AF, Butterbach-Bahl K, Dentener F, Stevenson D, Amann M, Voss M (2013) The global nitrogen cycle in the twenty-first century. Philos Trans R Soc Lond B Biol Sci **368:** 20130164

Frada MJ, Burrows EH, Wyman KD, Falkowski PG (2013) Quantum requirements for growth and fatty acid biosynthesis in the marine diatom Phaeodactylum tricornutum (Bacillariophyceae) in nitrogen replete and limited conditions. J Phycol **49:** 381-388

Gallardo L, Rhodes H (1997) Oxidized nitrogen in the remote pacific: the role of electrical discharges over the oceans. J. Atmos. Chem. **26:** 147-168

Gas E, Flores-Perez U, Sauret-Gueto S, Rodriguez-Concepcion M (2009) Hunting for plant nitric oxide synthase provides new evidence of a central role for plastids in nitric oxide metabolism. Plant Cell **21:** 18-23

Gerrard W (1980) Gas solubilities widespread applications. ,

Guerra LT, Levitan O, Frada MJ, Sun JS, Falkowski PG, Dismukes GC (2013) Regulatory branch points affecting protein and lipid biosynthesis in the diatom Phaeodactylum tricornutum. Biomass & Bioenergy **59:** 306-315

Holloway JM, Dahlgren RA (2002) Nitrogen in rock: Occurrences and biogeochemical implications. Global Biogechem. Cyc. **16:** 65-61–65-17.
Huang DW, Sherman BT, Tan Q, Kir J, Liu D, Bryant D, Guo Y, Stephens R, Baseler MW, Lane HC, Lempicki RA (2007) DAVID Bioinformatics Resources: expanded annotation database and novel algorithms to better extract biology from large gene lists. Nucleic Acids Research **35:** W169-W175
Ianora A, Miralto A (2010) Toxigenic effects of diatoms on grazers, phytoplankton and other microbes: a review. Ecotoxicology **19:** 493-511
IPCC (2014) Climate Change 2014: Synthesis Report. Contribution of Working Groups I, II and III to the Fifth Assessment Report of the Intergovernmental Panel on Climate Change. IPCC, Geneva, Switzerland
Jin CW, Du ST, Zhang YS, Lin XY, Tang CX (2009) Differential regulatory role of nitric oxide in mediating nitrate reductase activity in roots of tomato (Solanum lycocarpum). Ann Bot **104:** 9-17
Jouhet J, Marechal E, Bligny R, Joyard J, Block MA (2003) Transient increase of phosphatidylcholine in plant cells in response to phosphate deprivation. FEBS Lett **544:** 63-68
Kampschreur MJ, Temmink H, Kleerebezem R, Jetten MSM, van Loosdrecht MCM (2009) Nitrous oxide emission during wastewater treatment. Water Research **43:** 4093-4103
Keszler A, Zhang Y, Hogg N (2010) Reaction between nitric oxide, glutathione, and oxygen in the presence and absence of protein: How are S-nitrosothiols formed? Free Radic Biol Med **48:** 55-64
Kikkert JR (1993) The Biolistic(R) Pds-1000 He Device. Plant Cell Tissue and Organ Culture **33:** 221-226
Kohlwein SD (2010) Triacylglycerol homeostasis: insights from yeast. J Biol Chem **285:** 15663-15667
Kumar A, Castellano I, Patti FP, Palumbo A, Buia MC (2015) Nitric oxide in marine photosynthetic organisms. Nitric Oxide **47:** 34-39
Levitan O, Dinamarca J, Hochman G, Falkowski PG (2014) Diatoms: a fossil fuel of the future. Trends Biotechnol **32:** 117-124
Levitan O, Dinamarca J, Zelzion E, Gorbunov MY, Falkowski PG (2015) An RNA interference knock-down of nitrate reductase enhances lipid biosynthesis in the diatom Phaeodactylum tricornutum. Plant J **84:** 963-973
Levitan O, Dinamarca J, Zelzion E, Lun DS, Guerra LT, Kim MK, Kim J, Van Mooy BA, Bhattacharya D, Falkowski PG (2015) Remodeling of intermediate metabolism in the diatom Phaeodactylum tricornutum under nitrogen stress. Proc Natl Acad Sci U S A **112:** 412-417
Liu T, Zhang S, Chen J, Jiang K, Zhang Q, Guo K, Liu Y (2014) The transcriptional profiling of glycogenes associated with hepatocellular carcinoma metastasis. PLoS One **9:** e107941
Lowry OH, Rosebrough NJ, Farr AL, Randall RJ (1951) Protein Measurement with the Folin Phenol Reagent. Journal of Biological Chemistry **193:** 265-275
Mandal MK, Chandra-Shekara AC, Jeong RD, Yu K, Zhu S, Chanda B, Navarre D, Kachroo A, Kachroo P (2012) Oleic acid-dependent modulation of NITRIC OXIDE ASSOCIATED1 protein levels regulates nitric oxide-mediated defense signaling in Arabidopsis. Plant Cell **24:** 1654-1674
Marechal E, Block MA, Joyard J, Douce R (1994) Comparison of the kinetic properties of MGDG synthase in mixed micelles and in envelope membranes from spinach chloroplast. FEBS Lett **352:** 307-310
Marechal E, Block MA, Joyard J, Douce R (1994) Kinetic properties of monogalactosyldiacylglycerol synthase from spinach chloroplast envelope membranes. J Biol Chem **269:** 5788-5798
Marechal E, Miege C, Block MA, Douce R, Joyard J (1995) The catalytic site of monogalactosyldiacylglycerol synthase from spinach chloroplast envelope membranes. Biochemical analysis of the structure and of the metal content. J Biol Chem **270:** 5714-5722

Martens-Habbena W, Qin W, Horak RE, Urakawa H, Schauer AJ, Moffett JW, Armbrust EV, Ingalls AE, Devol AH, Stahl DA (2015) The production of nitric oxide by marine ammonia-oxidizing archaea and inhibition of archaeal ammonia oxidation by a nitric oxide scavenger. Environ Microbiol **17:** 2261-2274

Meï CE, Cussac M, Haslam RP, Beaudoin F, Wong YS, Marechal E, Rébeillé F (2017) C1 metabolism inhibition and nitrogen deprivation trigger triacylglycerol accumulation in Arabidopsis thaliana cell cultures and highlithgt a role of NPC in phosphatidylcholine-to-triacylglycerol pathway. . Front. Plant Sci.

Michalski G, Bhattachary SK, Girsh G (2014) NOx cycle and the tropospheric ozone isotope anomaly: an experimental examination. Atmos. Chem. Phys. **14:** 4935-4953

Miller MR, Megson IL (2007) Recent developments in nitric oxide donor drugs. Br J Pharmacol **151:** 305-321

Miller R, Wu G, Deshpande RR, Vieler A, Gartner K, Li X, Moellering ER, Zauner S, Cornish AJ, Liu B, Bullard B, Sears BB, Kuo MH, Hegg EL, Shachar-Hill Y, Shiu SH, Benning C (2010) Changes in transcript abundance in Chlamydomonas reinhardtii following nitrogen deprivation predict diversion of metabolism. Plant Physiol **154:** 1737-1752

Miralto A, Barone G, Romano G, Poulet SA, Ianora A, Russo GL, Buttino I, Mazzarella G, Laabir M, Cabrini M, Giacobbe MG (1999) The insidious effect of diatoms on copepod reproduction. Nature **402:** 173-176

Misra AN, Misra M, Singh R (2012) Chlorophyll fluorescence in plant biology. *In* AN Misra, ed, Biophysics. InTech, pp 171-192

Moreau M, Lee GI, Wang Y, Crane BR, Klessig DF (2008) AtNOS/AtNOA1 is a functional Arabidopsis thaliana cGTPase and not a nitric-oxide synthase. J Biol Chem **283:** 32957-32967

Moreau M, Lindermayr C, Durner J, Klessig DF (2010) NO synthesis and signaling in plants--where do we stand? Physiol Plant **138:** 372-383

Naqvi SWA, Yoshinari T, Jayakumar DA, Altabet MA, Narvekar PV, Devol AH, Brandes JA, Codispoti LA (1998) Budgetary and biogeochemical implications of N2O isotope signatures in the Arabian Sea. Nature **394:** 462-464

Nicholls JC, Davies CA, Trimmer M (2007) High-resolution profiles and nitrogen isotope tracing reveal a dominant source of nitrous oxide and multiple pathways of nitrogen gas formation in the central Arabian sea. Limnol. Oceanogr. **52:** 156-168.

Olasehinde EF, Takeda K, Sakugawa H (2010) Photochemical production and consumption mechanisms of nitric oxide in seawater. Environ. Sci. Technol. **44**

Pan Y, Ni BJ, Lu H, Chandran K, Richardson D, Yuan Z (2015) Evaluating two concepts for the modelling of intermediates accumulation during biological denitrification in wastewater treatment. Water Res **71:** 21-31

Ribalet F, Bastianini M, Vidoudez C, Acri F, Berges J, Ianora A, Miralto A, Pohnert G, Romano G, Wichard T, Casotti R (2014) Phytoplankton cell lysis associated with polyunsaturated aldehyde release in the Northern Adriatic Sea. PLoS One **9:** e85947

Ribalet F, Berges JA, Ianora A, Casotti R (2007) Growth inhibition of cultured marine phytoplankton by toxic algal-derived polyunsaturated aldehydes. Aquat Toxicol **85:** 219-227

Rockel P, Strube F, Rockel A, Wildt J, Kaiser WM (2002) Regulation of nitric oxide (NO) production by plant nitrate reductase in vivo and in vitro. J Exp Bot **53:** 103-110

Sakihama Y, Nakamura S, Yamasaki H (2002) Nitric oxide production mediated by nitrate reductase in the green alga Chlamydomonas reinhardtii: an alternative NO production pathway in photosynthetic organisms. Plant Cell Physiol **43:** 290-297

Sanchez-Calvo B, Barroso JB, Corpas FJ (2013) Hypothesis: Nitro-fatty acids play a role in plant metabolism. Plant Sci **199-200:** 1-6

Sanz-Luque E, Chamizo-Ampudia A, Llamas A, Galvan A, Fernandez E (2015) Understanding nitrate assimilation and its regulation in microalgae. Front Plant Sci **6:** 899

Sanz-Luque E, Ocana-Calahorro F, Llamas A, Galvan A, Fernandez E (2013) Nitric oxide controls nitrate and ammonium assimilation in Chlamydomonas reinhardtii. J Exp Bot **64:** 3373-3383
Siaut M, Heijde M, Mangogna M, Montsant A, Coesel S, Allen A, Manfredonia A, Falciatore A, Bowler C (2007) Molecular toolbox for studying diatom biology in Phaeodactylum tricornutum. Gene **406:** 23-35
Simionato D, Block MA, La Rocca N, Jouhet J, Marechal E, Finazzi G, Morosinotto T (2013) The response of Nannochloropsis gaditana to nitrogen starvation includes de novo biosynthesis of triacylglycerols, a decrease of chloroplast galactolipids, and reorganization of the photosynthetic apparatus. Eukaryot Cell **12:** 665-676
St Laurent CD, Moon TC, Befus AD (2015) Measurement of nitric oxide in mast cells with the fluorescent indicator DAF-FM diacetate. Methods Mol Biol **1220:** 339-345
Stohr C, Strube F, Marx G, Ullrich WR, Rockel P (2001) A plasma membrane-bound enzyme of tobacco roots catalyses the formation of nitric oxide from nitrite. Planta **212:** 835-841
Vardi A (2008) Cell signaling in marine diatoms. Commun Integr Biol **1:** 134-136
Vardi A, Bidle KD, Kwityn C, Hirsh DJ, Thompson SM, Callow JA, Falkowski P, Bowler C (2008) A diatom gene regulating nitric-oxide signaling and susceptibility to diatom-derived aldehydes. Curr Biol **18:** 895-899
Vardi A, Formiggini F, Casotti R, De Martino A, Ribalet F, Miralto A, Bowler C (2006) A stress surveillance system based on calcium and nitric oxide in marine diatoms. PLoS Biol **4:** e60
Varet H, Brillet-Gueguen L, Coppee JY, Dillies MA (2016) SARTools: A DESeq2- and EdgeR-Based R Pipeline for Comprehensive Differential Analysis of RNA-Seq Data. PLoS One **11:** e0157022
Vunjak-Novakovic G, Kim Y, Wu XX, Berzin I, Merchuk JC (2005) Air-lift bioreactors for algal growth on flue gas: Mathematical modeling and pilot-plant studies. Industrial & Engineering Chemistry Research **44:** 6154-6163
Wei L, Derrien B, Gautier A, Houille-Vernes L, Boulouis A, Saint-Marcoux D, Malnoe A, Rappaport F, de Vitry C, Vallon O, Choquet Y, Wollman FA (2014) Nitric oxide-triggered remodeling of chloroplast bioenergetics and thylakoid proteins upon nitrogen starvation in Chlamydomonas reinhardtii. Plant Cell **26:** 353-372
Wendehenne D, Pugin A, Klessig DF, Durner J (2001) Nitric oxide: comparative synthesis and signaling in animal and plant cells. Trends Plant Sci **6:** 177-183
Wilson ID, Neill SJ, Hancock JT (2008) Nitric oxide synthesis and signalling in plants. Plant Cell Environ **31:** 622-631
Yamasaki H, Sakihama Y (2000) Simultaneous production of nitric oxide and peroxynitrite by plant nitrate reductase: in vitro evidence for the NR-dependent formation of active nitrogen species. FEBS Lett **468:** 89-92
Yang J, Pan YF, Bowler C, Zhang LX, Hu HH (2016) Knockdown of phosphoenolpyruvate carboxykinase increases carbon flux to lipid synthesis in Phaeodactylum tricornutum. Algal Research-Biomass Biofuels and Bioproducts **15:** 50-58
Yoneda K, Yoshida M, Suzuki I, Watanabe MM (2016) Identification of a major lipid droplet protein in a marine diatom Phaeodactylum tricornutum. Plant Cell Physiol **57:** 397-406
Young MD, Wakefield MJ, Smyth GK, Oshlack A (2010) Gene ontology analysis for RNA-seq: accounting for selection bias. Genome Biol **11:** R14
Zehr JP, Ward BB (2002) Nitrogen cycling in the ocean: new perspectives on processes and paradigms. Appl Environ Microbiol **68:** 1015-1024
Zhang Z, Xing L, Wu Z, Liu C, Lin C, Liu L (2006) Discovery of nitric oxide in marine ecological system and the chemical characteristics of nitric oxide. Sci. Cina Ser. B Chem. **49:** 475-481
Zhu W, Xiao S, Zhang D, Liu P, Zhou H, Dai W, Liu F, Li H (2015) Highly efficient and stable Au/CeO2-TiO2 photocatalyst for nitric oxide abatement: potential application in flue gas treatment. Langmuir **31:** 10822-10830